NKS-498
ISBN 978-87-7893-596-0

# DISpersion of radioActivity fRom nuclear boMbs (DISARM) – final report

Jens Havskov Sørensen[1] (co-ordinator)
Kristian Holten Møller[1]
Kasper Skjold Tølløse[1]
Lennart Robertson[2]
Leif Å. Persson[3]
Daniel Vågberg[3]
Jan Pehrsson[4]
Henrik Roed[5]
Elias Pagh Senstius[5]
Naeem Ul Syed[6]
Anders Axelsson[7]
Anna Maria Blixt Buhr[7]
Jan Burman[3]
Jonas Lindgren[7]
Mikael Moring[8]
Tuomas Peltonen[8]
Mikko Voutilainen[8]

[1]Danish Meteorological Institute (DMI)
[2]Swedish Meteorological and Hydrological Institute (SMHI)
[3]Swedish Defence Research Agency (FOI)
[4]PDC-ARGOS
[5]Danish Emergency Management Agency (DEMA)
[6]Norwegian Radiation and Nuclear Safety Authority (DSA)
[7]Swedish Radiation Safety Authority (SSM)
[8]Radiation and Nuclear Safety Authority (STUK)

April 2025

## Abstract

The current geopolitical situation implies an increased risk of use of nuclear weapons, the detonation of which can imply atmospheric dispersion of radioactivity posing a risk to the public also at long distances from the detonation. Thus, there is a need for developing new, or improving existing, model prediction tools for such events aiming at enhanced civil protection. Accordingly, the overall intention with the DISARM project was to improve the capability of predicting the atmospheric dispersion of radioactivity from nuclear explosions.

The model system describes the initial spatial distribution of radioactive matter when stabilization has occurred around ten minutes after the detonation. This effective initial spatial distribution will be taken over by an operational atmospheric dispersion model.

Existing descriptions and parameterizations based on parameters observed in the field have been studied and improved by incorporating recently developed dependences on meteorological parameters.

An interface to nuclear decision-support systems has been developed. From either field observations of the geometry of the stabilized cloud, or from the yield in TNT equivalent as well as the height of burst, the interface calculates the parameters, which are required by the atmospheric dispersion model. These parameters are transferred to the dispersion model included in the request for dispersion calculation.

Previous NKS-B projects have demonstrated that inherent case-dependent meteorological uncertainties play a significant role for the atmospheric dispersion model results. Corresponding methods are developed and applied to selected cases in order to quantify the meteorological uncertainties of the predicted radioactive plumes from nuclear explosions.



## Key words

nuclear emergency preparedness, atmospheric dispersion modelling, nuclear weapons, detonation, stabilized cloud, particle size distribution

NKS-498
ISBN 978-87-7893-596-0
Electronic report, April 2025


NKS Secretariat
P.O. Box 49
DK - 4000 Roskilde, Denmark
Phone +45 4677 4041
www.nks.org
e-mail nks@nks.org

# DISpersion of radioActivity fRom nuclear boMbs (DISARM) – final report

## Final report of the NKS-B DISARM activity

## (Contract: AFT/B(24)1)

Jens Havskov Sørensen[1] (co-ordinator)
Kristian Holten Møller[1]
Kasper Skjold Tølløse[1]

Lennart Robertson[2]

Leif Å. Persson[3]
Daniel Vågberg[3]

Jan Pehrsson[4]

Agnieszka Hac-Heimburg[5]
Henrik Roed[5]
Elias Pagh Senstius[5]

Naeem Ul Syed[6]

Anders Axelsson[7]
Anna Maria Blixt Buhr[7]
Jan Burman[7]
Jonas Lindgren[7]

Mikael Moring[8]
Tuomas Peltonen[8]
Mikko Voutilainen[8]

[1]Danish Meteorological Institute (DMI)

[2]Swedish Meteorological and Hydrological Institute (SMHI)

[3]Swedish Defence Research Agency (FOI)

[4]PDC-ARGOS

[5]Danish Emergency Management Agency (DEMA)

[6]Norwegian Radiation and Nuclear Safety Authority (DSA)

[7]Swedish Radiation Safety Authority (SSM)

[8]Radiation and Nuclear Safety Authority (STUK)

# Table of contents

# Introduction

The current geopolitical situation indicates that there is an increased risk for use of weapons of mass destruction such as nuclear weapons. Detonation of nuclear weapons implies atmospheric dispersion of radioactivity posing a risk to the public also at longer distances from the detonation. Thus, there is a need for developing new, or improving existing, prediction model tools for such events aiming at enhanced civil protection. Accordingly, the overall intention with the DISARM project is to improve the capability to predict the atmospheric dispersion of radioactivity from detonation of nuclear bombs of different yields.

The envisioned model system will describe the initial spatial distribution of radioactive matter when stabilization has occurred around ten minutes after detonation. This effective initial spatial distribution will be taken over by an operational atmospheric dispersion model, which will have to be further developed in order to comply with such description.

The first version will be based on existing descriptions, e.g. the KDFOC3 approach by Harvey *et al.* (1992) in combination with the source strengths described by Kraus and Foster (2014), and using parameters which are observed in the field. It needs further to be considered if calculation of the effective initial distribution of radioactivity should ideally take place as a pre-processor implemented on the supercomputer at the national meteorological service or in the nuclear decision-support system (DSS) in use.

The system should preferably be able to accept NATO CBRN warning and reporting messaging according to the ATP-45 standard (NATO, 2020). Algorithms converting the information contained in these messages to the inputs are needed for the atmospheric dispersion models. This may include merging and co-processing of multiple observation reports.

The description of the initial phase can be improved, e.g. by incorporating dependences on meteorological parameters and arriving at better descriptions of particle size distributions. Here, recent work by Arthur *et al.* (2021) on the early dynamics of the nuclear cloud may be of interest; however, this approach does not take into account the fireball interaction with ground.

The previous NKS-B projects MUD, MESO and AVESOME have demonstrated that inherent case-dependent meteorological uncertainties play a significant role for the atmospheric dispersion model results. As for nuclear power plants, also uncertainties of the source term description are expected to be important; however, as the meteorological uncertainties influence the transport pathway they may well have significant impact on emergency preparedness far from the detonation. In DISARM, methods will be developed and applied to quantify the meteorological uncertainties of the predicted plumes.

A possible release scenario is a nearly simultaneous detonation of a number of nuclear weapons at more or less the same location. However, in such a case one might not have field observations available of the individual stabilized clouds for each detonation due to overlapping mushroom clouds. In such a case, the stabilized cloud observed is likely to be the result of all of these explosions and will thus be treated as a single joint cloud by the atmospheric dispersion model in use for civilian emergency preparedness.

## NATO Message Standards for Nuclear Weapon Detonation

Information from military sources on detonation of a nuclear weapon is likely to be transmitted as NATO CBRN standard messages, e.g. as described in the ATP-45 publication. Such messages may include field observations of date and time and geographic coordinates of the detonation(s), the number of detonations, as well as the nature of the burst and parameters describing the initial spatial distribution of the radioactive cloud after stabilization, around five to ten minutes after the explosion. It is thus desirable that the nuclear decision-support system in use is capable of parsing NATO CBRN messages. ARGOS is able to read certain such messages; however, an update is needed. In the near future, ARGOS will also be able to create ATP-45 messages to be used by ATP-45 compliant systems.

## Artificial Cases

Hypothetical battlefield scenarios are prepared involving a 100 kt detonation over the Swedish Hagshult airbase. The UTM coordinates are given as UTM Zone 33, Easting 47983, Northing 50242, which is equivalent to MGRS coordinates 33V VD 47983 50242, and to geographical coordinates (57.2921°N, 14.1369°E). Two meteorological situations were selected, one involving anti-cyclonic conditions with subsidence, dry weather and low wind speeds, another involving cyclonic conditions with rising air, precipitation and windy conditions. For the two cases, corresponding deterministic Harmonie NWP model forecast data from both the DMI and the SMHI Harmonie versions were derived for the atmospheric dispersion calculations. In addition, ensemble-statistical NWP model data of the DMI Harmonie system have been obtained for the selected cases.

## Operational Atmospheric Dispersion Models

### Danish Emergency Response Model of the Atmosphere (DERMA)

The Danish Emergency Response Model of the Atmosphere (DERMA) (Sørensen *et al.*, 2007; Sørensen, 1998) is a comprehensive numerical regional and meso-scale atmospheric dispersion model developed at the Danish Meteorological Institute (DMI). The model is used operationally for the Danish nuclear emergency preparedness, for which the Danish Emergency Management Agency (DEMA) is responsible (Hoe *et al.*, 2002). The model is also employed for veterinary emergency preparedness (Sørensen *et al.*, 2000; 2001; Mikkelsen *et al.*, 2003; Gloster *et al.*, 2010a; 2010b), where it is used for assessment of airborne spread of animal diseases, e.g. foot-and-mouth disease. DERMA may also be used to simulate atmospheric dispersion of chemical substances, biological warfare agents and ashes from volcanic eruptions, and it has been employed for probabilistic nuclear risk assessment for nuclear reactor accidents (Lauritzen *et al.*, 2006; 2007; Baklanov *et al.*, 2003; Mahura *et al.*, 2003; 2005).

The main objective of DERMA is to predict the dispersion of a radioactive plume and the accompanied deposition. However, the model may also be used in situations where increased levels of radioactivity have been measured but no information is available on a radioactive release. In such cases, inverse (adjoint) modelling may be applied whereby potential sources of radioactivity may be localised and release rates estimated.

The three-dimensional model is of Lagrangian type making use of a hybrid stochastic particle-puff diffusion description, and it is currently capable of describing plumes at downwind distances up to the global scale (Sørensen *et al.*, 1998). The model utilizes aerosol size dependent dry and wet deposition parameterisations as described by Baklanov and Sørensen (2001).

Currently, DERMA makes use of analysed and forecasted meteorological data of various deterministic versions at DMI of the NWP model Harmonie (Bengtsson *et al.*, 2017) covering North-western Europe, Greenland and the Faeroes, and from the global model developed and operated by the European Centre for Medium-range Weather Forecasts (ECMWF). Furthermore, DERMA utilizes the COMEPS ensemble prediction system, which is based on the Harmonie model.

### Description of Stabilized Cloud

Because of the energy released on detonation, nuclear explosions close to the surface form characteristic mushroom shaped clouds. These clouds contain radioactive material which will be dispersed in the atmosphere. To model the atmospheric dispersion as accurately as possible, we need to be able to approximate the initial three-dimensional structure of the stabilized mushroom cloud to serve as a starting point for our atmospheric dispersion model.

The initial description of the stabilized cloud for the DERMA code is based on the "K-Division Defense Nuclear Agency Fallout Code" (KDFOC3, Harvey *et al.*, 1992). In this description, the stabilized cloud can be approximated as a cylindrical main cloud, a tapered stem and an optional cylindrical base surge, whose presence depends on the altitude of detonation. Given the yield and altitude of detonation, KDFOC3 can provide a full empirical description of the stabilized cloud. Via the decision support program ARGOS, the Danish Emergency Management Agency (DEMA) provides this input to generate the KDFOC3 description of the stabilized cloud. However, additional flexibility is built into the system to allow modifications beyond the KDFOC3 description based on e.g. observations. This includes potential gaps between the different parts of the cloud (main, stem and base surge). Additionally, the KDFOC3 description is extended to allow for free air bursts (i.e. explosions without significant interaction with the surface), which is not originally included in the description.

Based on the input from DEMA, ARGOS provides DERMA with the following nine geometrical parameters which fully describe the stabilized cloud within the implemented framework:

- Radius of the main cloud
- Altitude of the top of the main cloud
- Altitude of the bottom of the main cloud
- Altitude of the top of the stem
- Altitude of the bottom of the stem
- Radius of the top of the stem
- Radius of the bottom of the stem
- Height of the base surge (if present)
- Radius of the base surge (if present)

In addition, ARGOS provides the following required for modeling of the initial state:

- Latitude and longitude of detonation
- Time of formation of the stabilized cloud (postulated to be 10 minutes after detonation)
- Source term specifying the (pseudo)nuclides and activity

For the dispersion modelling, the stabilized cloud is described by a set of identical spheroids distributed in three-dimensional space. Initially, based on the geometrical parameters received, a two dimensional structure of the cloud is generated showing the radius of the cloud as a function of altitude, Figure 1. Radii smaller than the spheroid radius are modelled as the spheroid radius. This continuous description is discretized by dividing the structure into a number of vertical layers, each with a fixed separation of 20 m. In each vertical layer, the spheroids are distributed based on closest packing to best reproduce the radius of the cloud at the given altitude, Figure 2. Each alternating layer is rotated by 30 degrees relative to each other to better represent the overall circular geometry. The centers of the spheroids are separated by a distance related to the grid size of the meteorological model used for the simulation and thus varies from model to model.

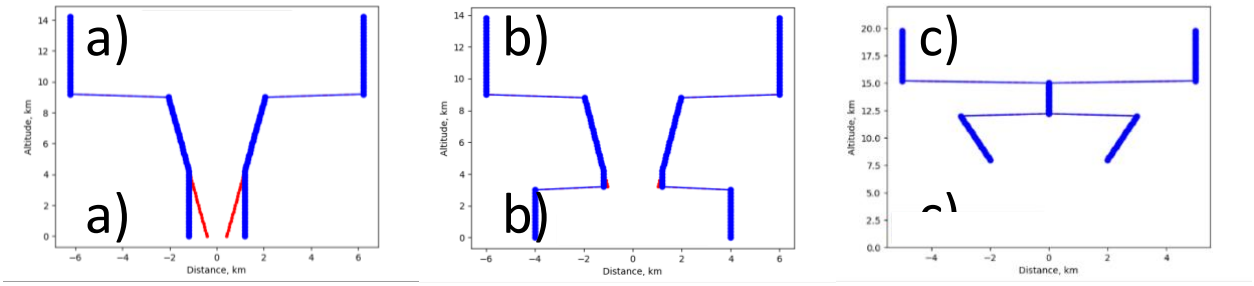


**Figure 1** Illustration of the altitude-radius structure of three modelled clouds: a) the KDFOC3 description of the stabilized cloud from detonation of a 100 kt nuclear device, b) a comparable cloud but including a base surge, and c) a non-continuous cloud not reaching the surface representing a free air burst. Red shows the desired radius and blue the actually modelled radius, which is limited by the spheroid radius.

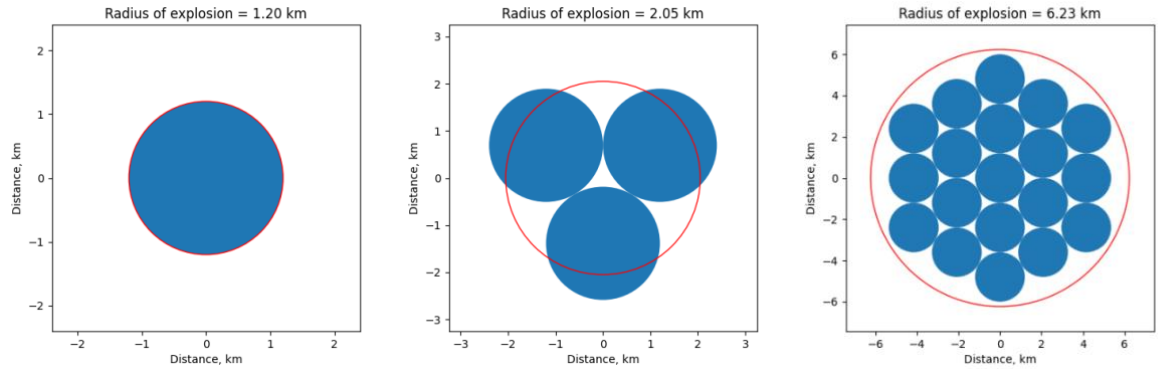


**Figure 2** Examples of the closest packing of circles in the bottom of the stem (left), the top of the stem (middle) and the main cloud (right) of the mushroom cloud shown in panel a) of Figure 1 Illustration of the altitude-

radius structure of three modelled clouds: a) the KDFOC3 description of the stabilized cloud from detonation of a 100 kt nuclear device, b) a comparable cloud but including a base surge, and c) a non-continuous cloud not reaching the surface representing a free air burst. Red shows the desired radius and blue the actually modelled radius, which is limited by the spheroid radius.Figure 1.

The total activity is distributed vertically in the cloud according to Rolph *et al.* 2014, based on Heffter (1969). Specifically, the stem and main cloud are each divided into three parts, each part containing a fixed amount of the total activity. From the bottom-up, this distribution is [2.5, 5, 15, 30, 30, 17.5]%. Within each of these six sections of the cloud, the activity is distributed evenly between all puffs, translating to a homogeneous distribution horizontally, cf. Figure 3 and Figure 4.

If a base surge is present, this is given a fixed fraction of the total activity of 20% (Knox, 1964). For free air bursts without stems and base surges, the activity is distributed evenly in the whole cloud.

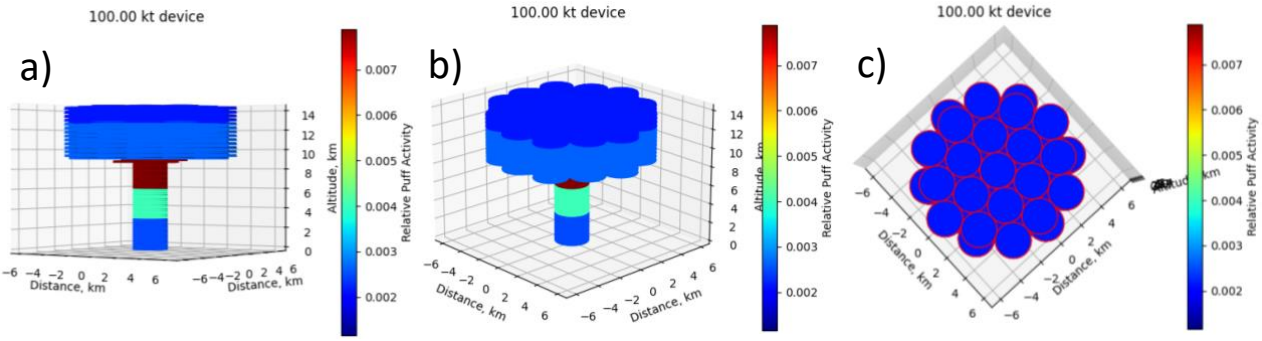


**Figure 3** Different views of the three-dimensional structure of cloud a) in Figure 1 Illustration of the altitude-radius structure of three modelled clouds: a) the KDFOC3 description of the stabilized cloud from detonation of a 100 kt nuclear device, b) a comparable cloud but including a base surge, and c) a non-continuous cloud not reaching the surface representing a free air burst. Red shows the desired radius and blue the actually modelled radius, which is limited by the spheroid radius.. For the top view, c), the spheroids are outlined in red for visual clarity. Each spheroid is represented as a cylinder of uniform activity for this visualization.

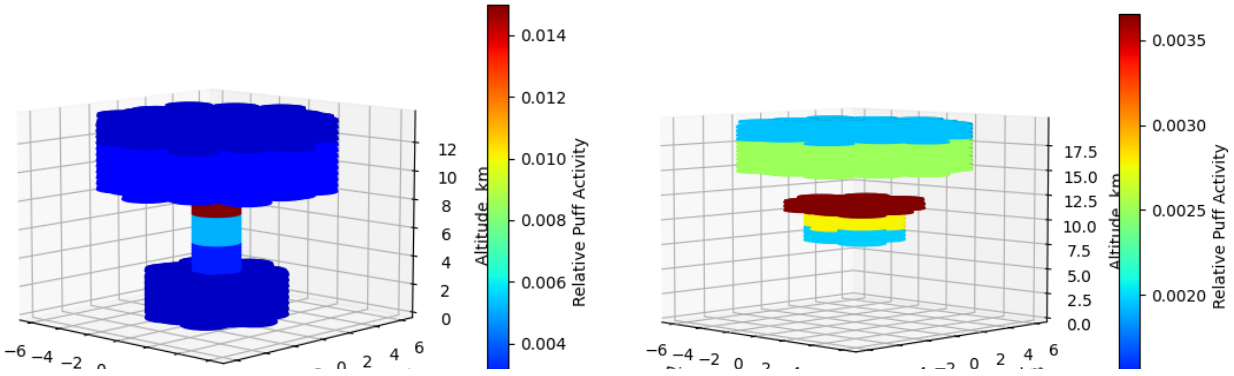


**Figure 4** Three dimensional structures of the clouds b) and c) in Figure 1 Illustration of the altitude-radius structure of three modelled clouds: a) the KDFOC3 description of the stabilized cloud from detonation of a 100 kt nuclear device, b) a comparable cloud but including a base surge, and c) a non-continuous cloud not reaching the surface representing a free air burst. Red shows the desired radius and blue the actually modelled radius, which is limited by the spheroid radius.**Error! Reference source not found.**.

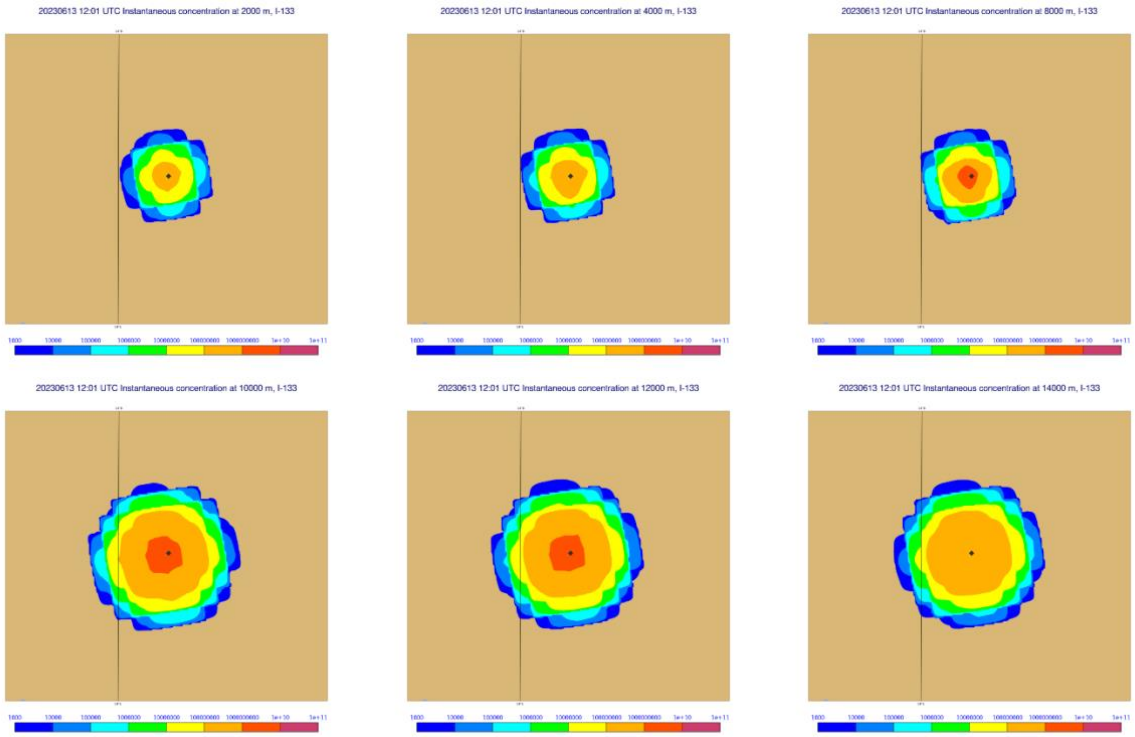


**Figure 5** Horizontal cross-sections at different heights in DERMA one minute after stabilisation of the cloud resulting from a detonated 100 kt nuclear device as shown in a) in Figure 1 Illustration of the altitude-radius structure of three modelled clouds: a) the KDFOC3 description of the stabilized cloud from detonation of a 100 kt nuclear device, b) a comparable cloud but including a base surge, and c) a non-continuous cloud not reaching the surface representing a free air burst. Red shows the desired radius and blue the actually modelled radius, which is limited by the spheroid radius.. The six panels (from top left) correspond to the six activity bins outlined in the text from the bottom and upwards: Each third of the stem (top row) and main cloud (bottom row). The small black diamond represents the point of detonation.

## Application to Selected Cases

The mushroom cloud shown in part a) in Figure 1, and in 3D in Figure 3, and Figure 4 is used as the initial condition for two independent DERMA runs on two dates with very different weather conditions. The dispersion with DERMA is modelled using meteorological data from the HARMONIE-Arome model. Specifically, the models are run with the NEA domain, Figure 6, with a horizontal resolution of about 2.5 km. The NEA domain covers Northern Europe including Iceland. The models are run until no further change is observed in the modelled airborne and deposited activity. The simulations assume detonation of a 100 kt nuclear device at the surface of the Hagshult airbase in Sweden (latitude: 57.29219°N, longitude: 14.13693°E). The source term used for the nuclear detonation modelling shown in the above figures is a non-decaying pseudo-nuclide labelled Ps-1 with a modelled activity of about $1.7 \times 10^{19}$ Bq/s released in a period of 60 seconds. In the future operational set-up, this value will be provided by the user of the nuclear decision-support system.

The two meteorological cases modelled are:

Case 1: June 13, 2023, 12.00: Stable, warm summer day with low wind.

Case 2: August 8, 2023, 09.00: The storm Hans with strong wind.

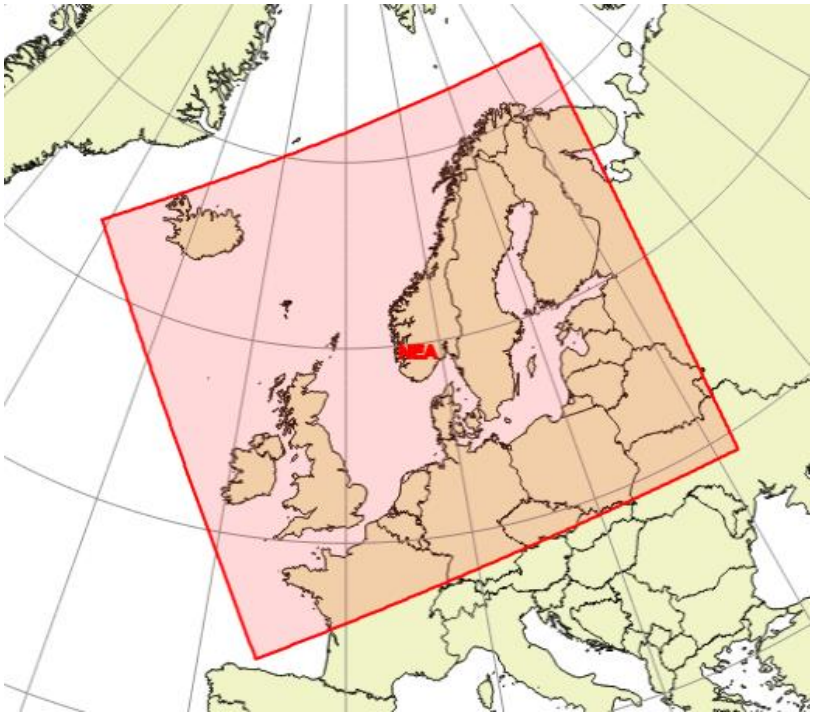


**Figure 6** The NEA version of the Harmonie Numerical Weather Prediction (NWP) model covering the Northern Europe and Iceland.

### *Case 1: June 13, 2023*

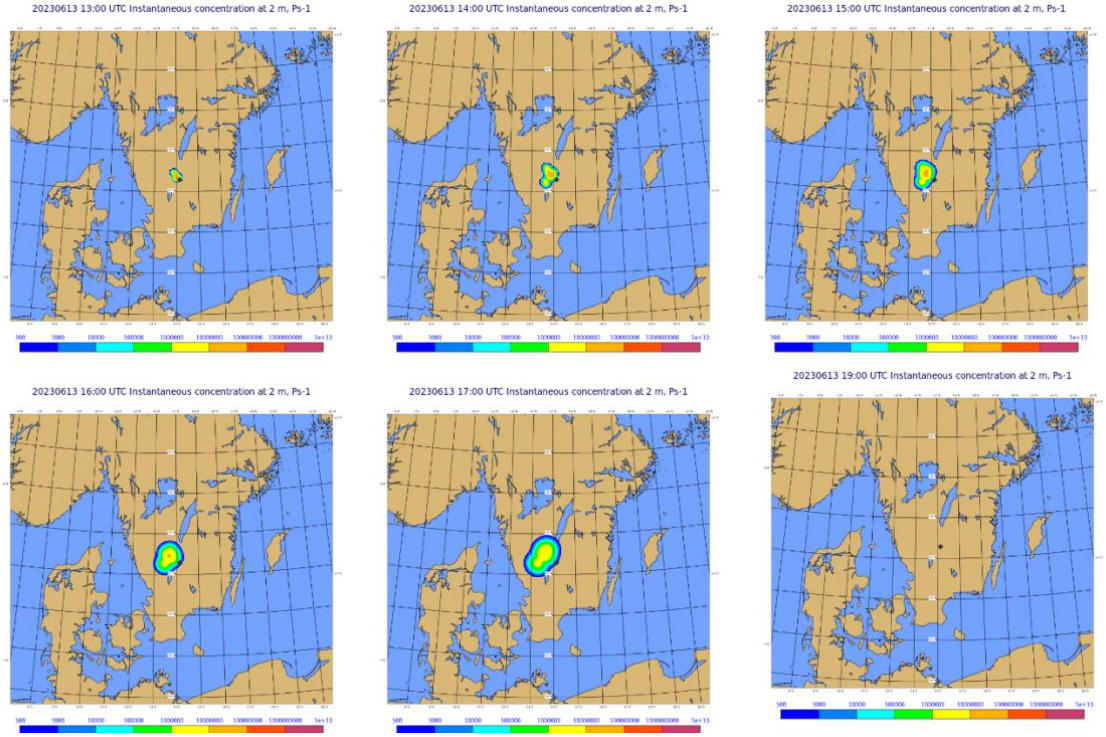


**Figure 7** Instantaneous air activity (Bq/m$^3$) at 2 m height at selected times following detonation of a 100 kt nuclear device at Hagshult Airbase (black diamond) on June 13, 2023 at 12.00. The modelling was continued until no further changes were observed.

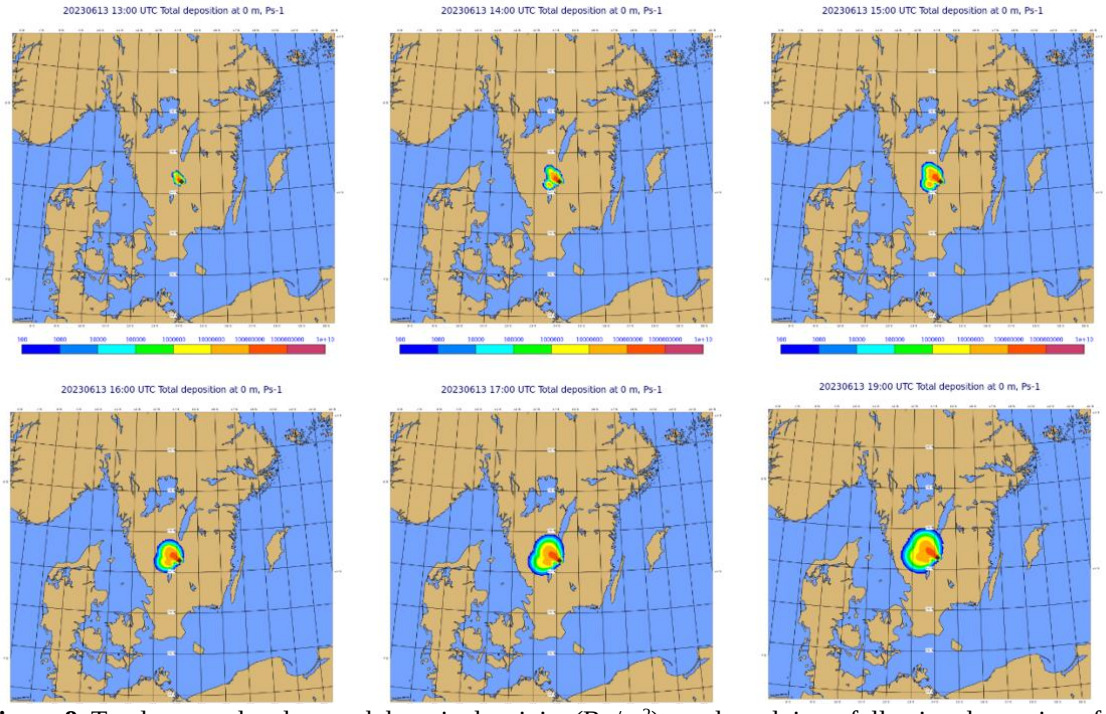


**Figure 8** Total accumulated ground deposited activity (Bq/m$^2$) at selected times following detonation of a 100 kt nuclear device at Hagshult Airbase (black diamond) on June 13, 2023 at 12.00. The modelling was continued until no further changes were observed.

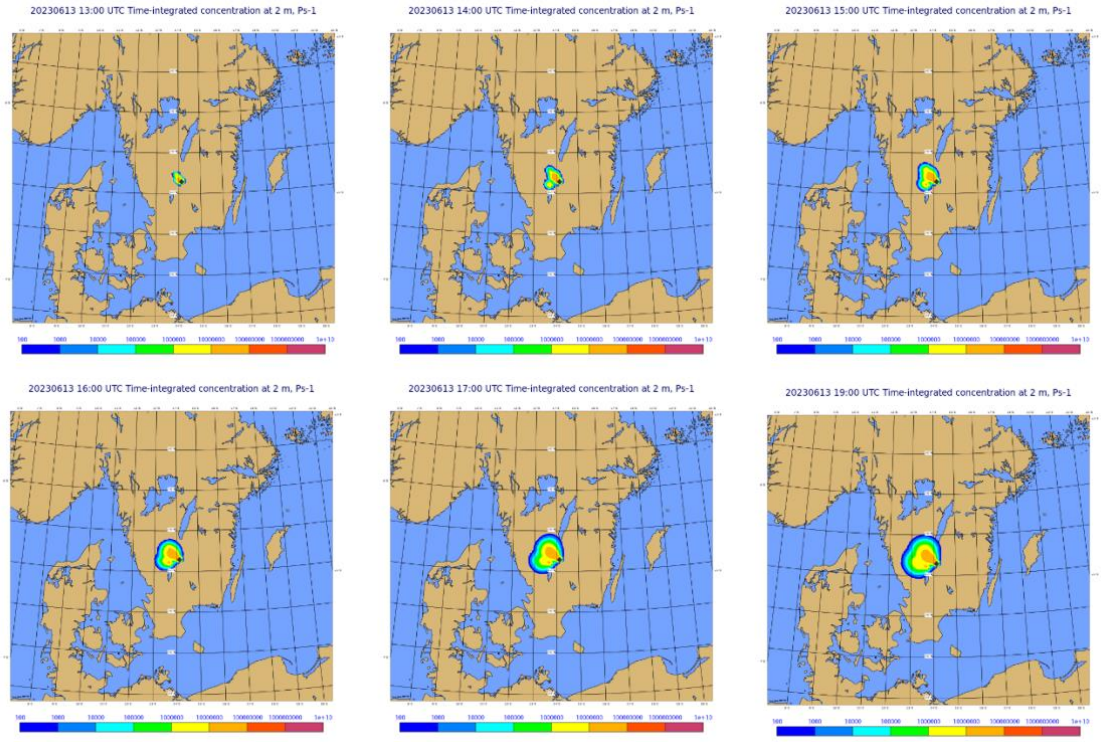


**Figure 9** Time-integrated air activity (Bq h/m$^3$) at 2 m height at selected times following detonation of a 100 kt nuclear device at Hagshult Airbase (black diamond) on June 13, 2023 at 12.00. The modelling was continued until no further changes were observed.

### *Case 2: August 8, 2023*

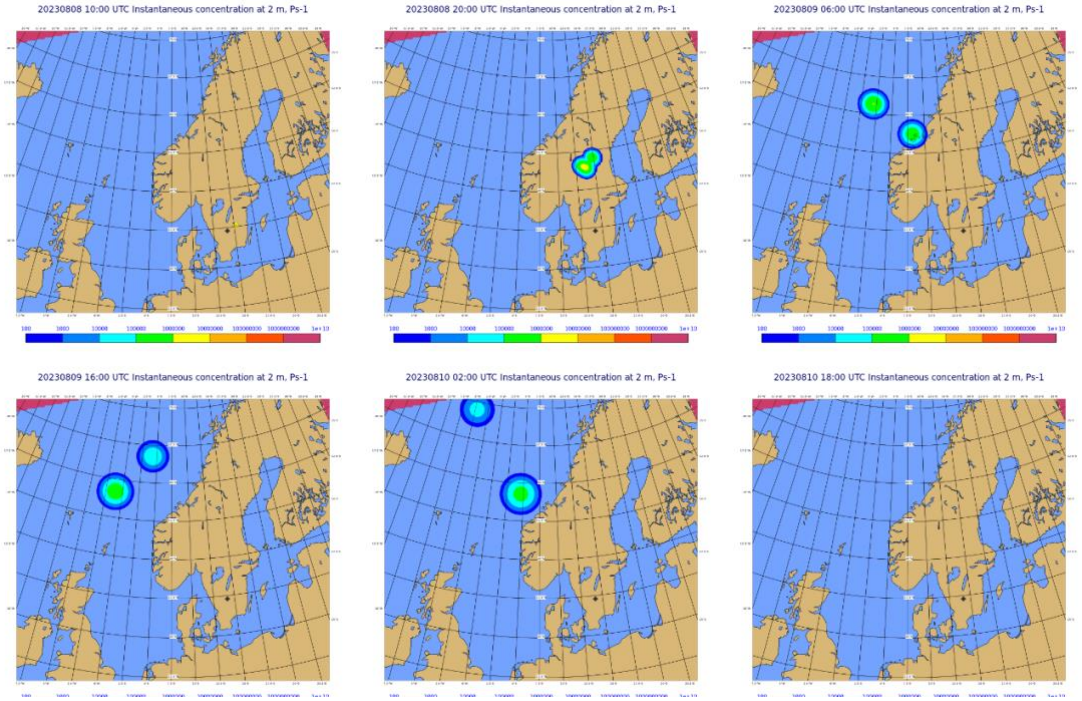


**Figure 10** Instantaneous air activity (Bq/m$^3$) at 2 m height at selected times following detonation of a 100 kt nuclear device at Hagshult Airbase (black diamond) on August 8, 2023 at 09.00. The modelling was continued until no further changes were observed. The red artifacts in the upper corners show the edge of the meteorological model.

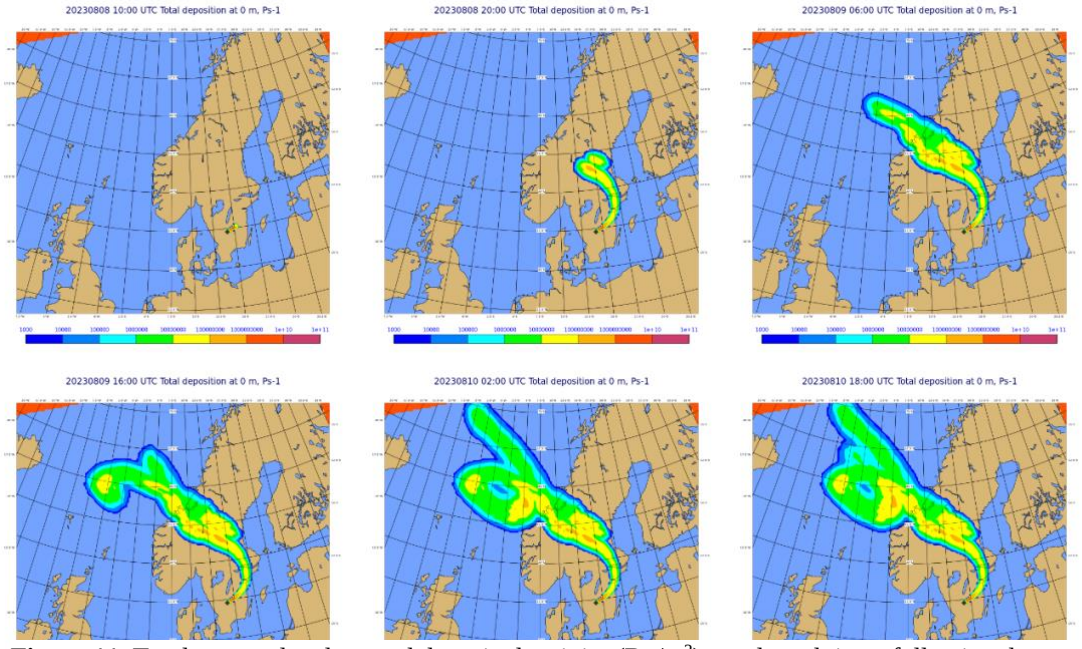


**Figure 11** Total accumulated ground deposited activity (Bq/m$^2$) at selected times following detonation of a 100 kt nuclear device at Hagshult Airbase (black diamond) on August 8, 2023 at 09.00. The modelling was continued until no further changes were observed. The red artifacts in the upper corners show the edge of the meteorological model.

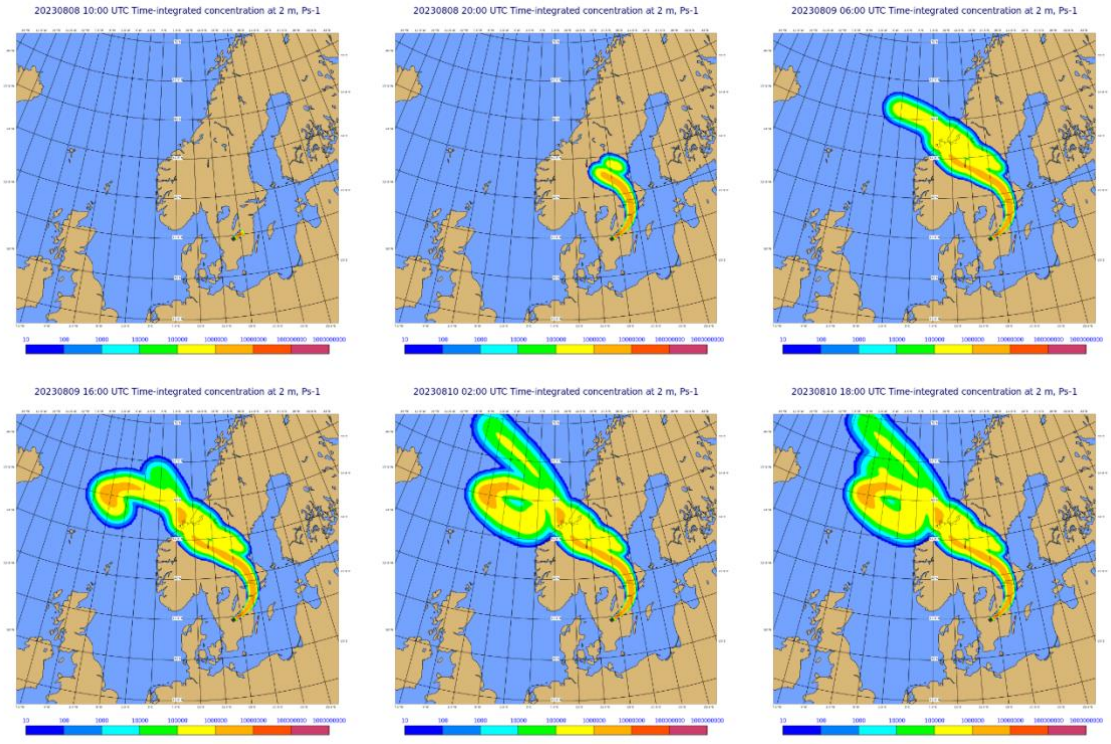


**Figure 12** Time-integrated air activity (Bq h/m$^3$) at 2 m height at selected times following detonation of a 100 kt nuclear device at Hagshult Airbase (black diamond) on August 8, 2023 at 09.00. The modelling was continued until no further changes were observed.

## The Meteorological Ensemble

The meteorological forcings used for the dispersion modeling are based on output from the DINI-EPS ensemble, which is currently in operation at United Weather Centres West (UWC-W). The ensemble consists of 30+1 ensemble members calculated using the non-hydrostatic Harmonie numerical weather prediction (NWP) model (Bengtsson *et al.,* 2017). The ensemble is lagged with the so-called control member being calculated every hour, along with five of the 30 perturbed members. Each run has a forecast length of 60 hours, resulting in 54 hours of forecast with all members overlapping. The ensemble employs simultaneous perturbations to the data assimilation, lateral boundary conditions as well as selected parameters of the surface and model parametrizations.

Output from the global NWP model of the ECMWF, the Integrated Forecasting System (IFS), is used to describe the lateral boundary conditions. Specifically, IFSHRES is used for the control member, while each of the perturbed members use boundary conditions from a separate member of the IFSENS ensemble.

Five selected physical parameters governing the behavior of parametrized atmospheric (sub)processes are perturbed using the Stochastically Perturbed Parametrizations scheme (SPP, Ollinaho 2017). Similarly, six different surface parameters are perturbed for the different ensemble members (Bouttier *et al.,* 2016).

The NWP output used for our dispersion modeling covers the NEA domain shown in Figure 6 with a horizontal resolution of 0.022 degrees, corresponding to about 2.5 km. The model employs 90 vertical levels with uneven spacing, increasing with increasing altitude.

### *Emission scenarios*

For comparison, we run two emission scenarios, one corresponding to the detonation of a nuclear device and one corresponding to an accident at a nuclear power plant. Both emission scenarios start at the same time (see “Meteorological Cases” below) and location. The location of the emissions is the Hagshult Airbase in southern Sweden (latitude: 57.2922°, longitude: 14.1369°).

#### Nuclear Weapon detonation (NW)

The nuclear weapon detonation scenario is modelled as a surface detonation of a 100 kt nuclear device. In the KDFOC3 description employed here, this results in a mushroom cloud with a total height of 14.37 km and a main cloud radius of 6.23 km. A visual representation of the mushroom cloud is given in Figure 13, and the full set of KDFOC3 parameters are given in Table 1.

The emission from the nuclear device is modelled with a single non-decaying pseudo-nuclide labelled Ps-1. The pseudo-nuclide can be considered a tracer for the activity from which the actual activity can subsequently be calculated using either empirical relations or the application of a (time-dependent) nuclide vector. As such, for this report, we present the activity of the pseudo-nuclide with a unit of pseudo-Becquerels (pBq) to distinguish it from an actual activity. The stabilized mushroom cloud is modelled to have a duration of one minute, with an emission rate of $1.6935 \cdot 10^{19}$ pBq/s for that period resulting in a total activity

of $1.0 \cdot 10^{21}$ pBq released. The dispersion is modelled for up to a total time of 48 hours after detonation.

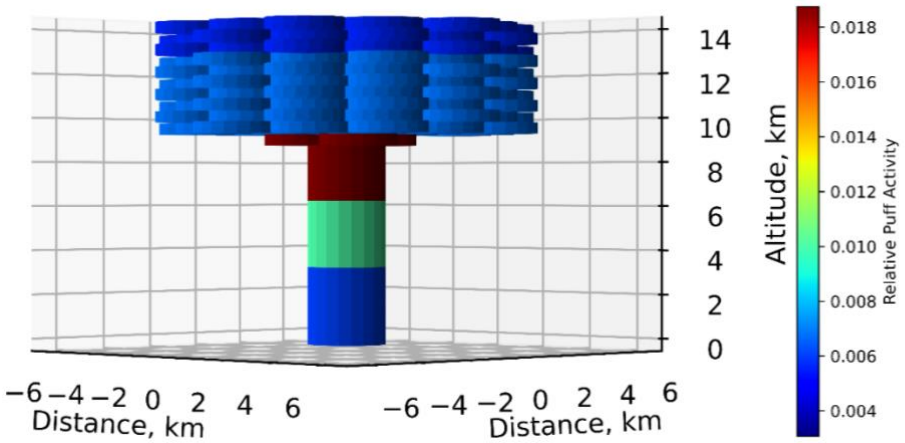


**Figure 13** Illustration of the mushroom cloud resulting from a 100 kt surface detonation within the KDFOC3 framework as implemented in the DERMA model system. For clarity, the puffs are visualized as cylinders of 500 m height, while they are actually modelled with a Gaussian distribution and separated by only 20 m vertically. The colors represent the relative puff activity.

**Table 1** KDFOC3 parameters for a 100 kt surface detonation as modelled in this study.

| Parameter | Value (km) |
|---|---|
| Altitude of top of main cloud | 14.37 |
| Altitude of bottom of main cloud | 9.15 |
| Radius of main cloud | 6.23 |
| Radius of top of stem | 2.08 |
| Radius of bottom of stem | 0.417 |
| Altitude of top of stem | 9.15 |
| Altitude of bottom of stem | 0.0 |
| Altitude of top of base surge | 0.0 |
| Radius of base surge | 0.0 |

### Nuclear Power Plant accident (NPP)

The source term for the emission scenario intended to simulate an accident at a nuclear power plant is taken from the NKS project "Added Value of uncertainty Estimates of SOurce term and Meteorology (AVESOME)", cf. Sørensen *et al.* (2019). We chose an emission scenario corresponding to a severe case, specifically, a core meltdown from the reactor hall with unfiltered bypass release, i.e. the source term labelled "BYP-RH" in AVESOME.

The source term corresponds to a continuous emission of radionuclides over a total period of 48 hours. The source term contains the following isotopes: Rb-88, Mo-99, Te-132, I-131, Xe-133 and Cs-137. The emission occurs in four distinct phases each having its own emission rate of the six different radionuclides. The total activity released over the period of 48 hours is of $6.0 \cdot 10^{18}$ Bq. Details of the four phases and their emission rates are given in Table 2. The release is modelled to occur at an altitude of 49 meters above ground.

**Table 2**. Details of the emission rates of the different radioisotopes in each of the four phases for the modelled emission following an accident at a nuclear power plant, based on the emission scenario "BYP-RH" in the NKS-project AVESOME.

| **Phase** | **1** | **2** | **3** | **4** |
|---|---|---|---|---|
| Start time (hours after accident) | 0 | 10.66 | 13.33 | 19.25 |
| Duration (hours) | 10.66 | 2.66 | 5.92 | 28.75 |
| Rb-88 emission rate of (Bq/s) | $1.28 \cdot 10^{13}$ | $4.99 \cdot 10^{12}$ | $3.34 \cdot 10^{12}$ | $7.62 \cdot 10^{10}$ |
| Mo-99 emission rate of (Bq/s) | $1.73 \cdot 10^{13}$ | $2.58 \cdot 10^{13}$ | 0.0 | 0.0 |
| Te-132 emission rate of (Bq/s) | $2.05 \cdot 10^{13}$ | $1.65 \cdot 10^{13}$ | $3.63 \cdot 10^{12}$ | $3.77 \cdot 10^{11}$ |
| I-131 emission rate of (Bq/s) | $1.71 \cdot 10^{13}$ | $1.32 \cdot 10^{13}$ | $1.71 \cdot 10^{12}$ | $3.71 \cdot 10^{11}$ |
| Xe-133 emission rate of (Bq/s) | $6.12 \cdot 10^{13}$ | $1.11 \cdot 10^{13}$ | 0.0 | 0.0 |
| Cs-137 emission rate of (Bq/s) | $2.31 \cdot 10^{12}$ | $9.02 \cdot 10^{11}$ | $6.06 \cdot 10^{11}$ | $1.38 \cdot 10^{10}$ |

### *Meteorological cases*

Three different meteorological cases have been selected, and the DINI-EPS Harmonie ensemble prediction system has been applied to all three. For a analysis given time, each of the 31 ensemble members have 54 hours of overlapping forecast. The times given for each case represent the time of the start of emission, which is offset from the start of the forecast by 4–8 hours.

#### September 12, 2024, 16.00 UTC

The period is characterized by a high-pressure system starting in the western Atlantic but slowly moving eastwards towards the emission site, with a low-pressure region north of Norway. At the same time, another high-pressure area is located above the western part of Russia. The wind at the emission site in Southern Sweden starts out from a southerly direction, but gradually moves over westerly to a northern direction during the simulation. The typical wind speed at an altitude of 10 m is about 3–5 m/s. In general, the wind speed increases with height; in this case up to around 50 m/s at 9 km above ground (300 hPa).The period is relatively dry, with a few smaller showers passing the area of interest, due to the influence from the low-pressure system over the Norwegian Sea.

#### October 10, 2024, 08.00 UTC

At the start of the simulation, the low-pressure system associated with the storm Kirk (remnant of the tropical hurricane of the same name) is located over southern Denmark. The system gradually moves in a northeasterly direction, passing the emission site. This results in westerly winds at the emission site and winds that are more southerly over the Baltic Sea. The low-pressure system also results in precipitation passing the emission site during simulation.

#### October 24, 2024, 16.00 UTC

This case is governed by a high-pressure system located over central Europe with a corresponding low-pressure system northwest of Norway moving east. The winds in southern Sweden are largely southerly and southwesterly during the simulation period. Near the end of the emission, small showers are present near the emission site.

### *Results*

For each combination of the two emission scenarios and the three meteorological cases, we run DERMA simulations for all members of the DINI-EPS ensemble and calculate ensemble statistics. The results are shown for the final time step in common between the two simulations. For the nuclear-weapon modeling, the pseudo-nuclide concentration and deposition are shown, and for the nuclear power plant accident modeling, values for Cs-137 are shown.

September 12, 2024, 16.00 UTC

| Emission | 10th percentile | 50th percentile | 90th percentile |
|---|---|---|---|
| NW | 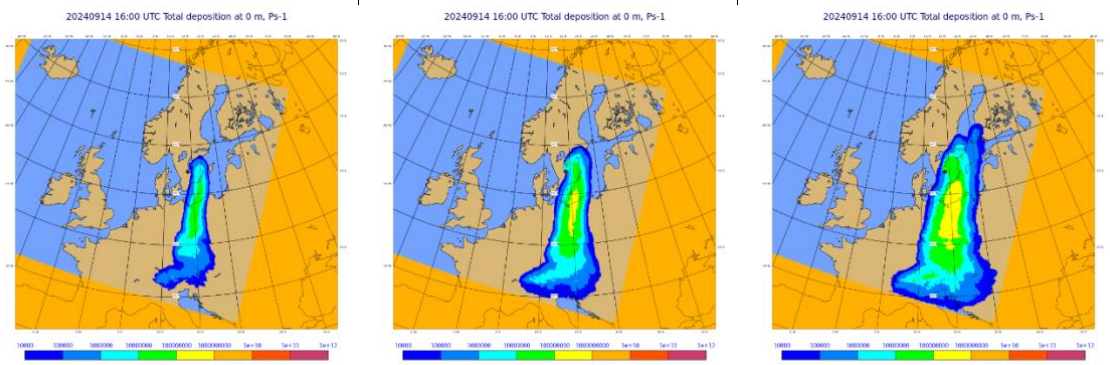  | | |
| NPP | 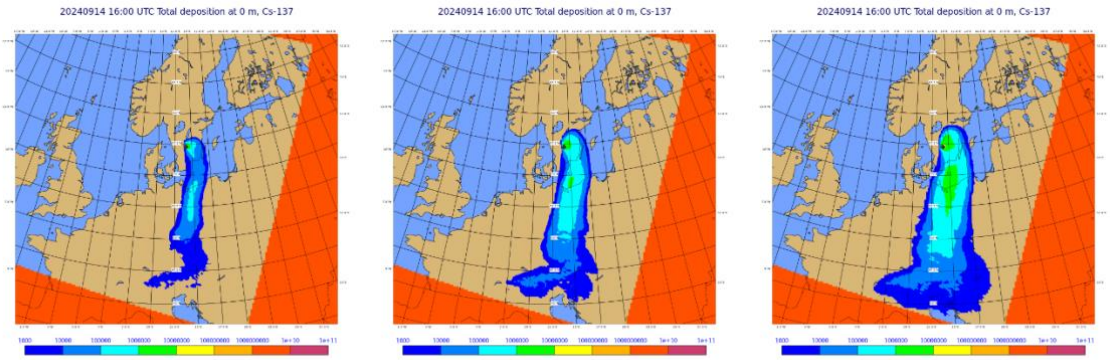  | | |

**Figure 14** 10th, 50th and 90th percentile of total accumulated ground deposited activity (pBq/ $m^2$ or Bq/$m^2$) at the end of simulation following either simulated detonation of a 100 kt nuclear device (NW) or simulated nuclear power plant accident (NPP) at Hagshult Airbase (black diamond) on September 12, 2024 at 16.00 UTC. The colored box surrounding the figures show the outline of the NWP domain.

| Emission | 10th percentile | 50th percentile | 90th percentile |
|---|---|---|---|
| NW | 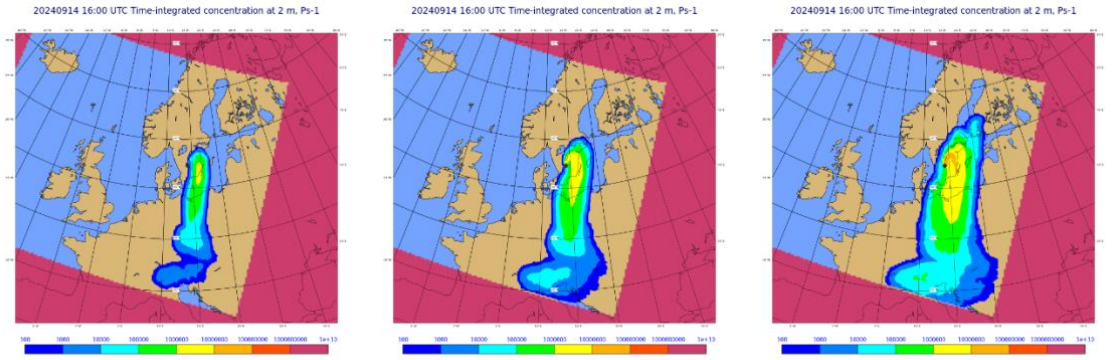  | | |
| NPP | 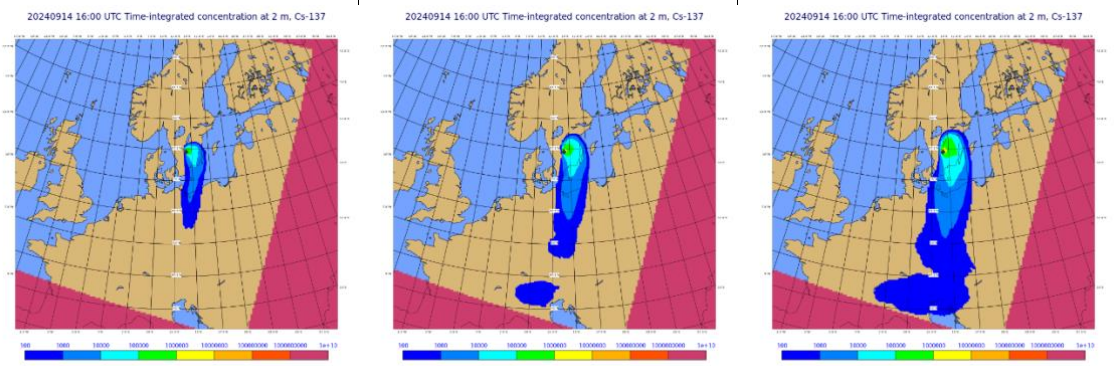  | | |

**Figure 15** 10th, 50th and 90th percentile of time-integrated air activity (pBq h/m$^3$ or Bq h/m$^3$) at 2 m height at the end of simulation following either simulated detonation of a 100 kt nuclear device (NW) or simulated nuclear power plant accident (NPP) at Hagshult Airbase (black diamond) on September 12, 2024 at 16.00 UTC. The colored box surrounding the figures show the outline of the NWP domain.

| NW | NPP |
| --- | --- |
| 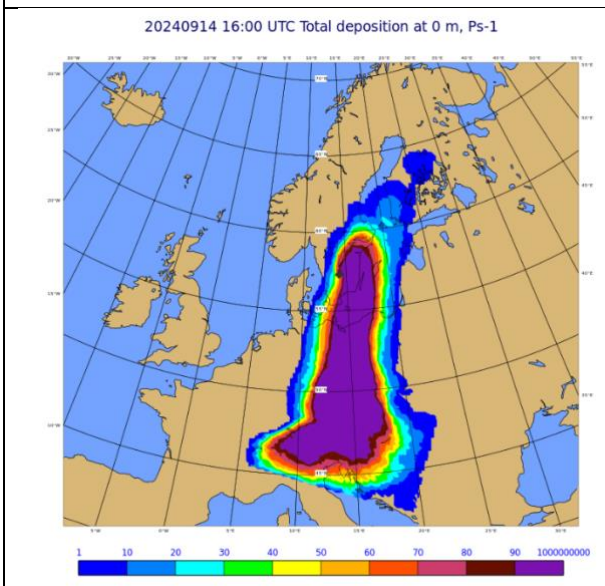  | 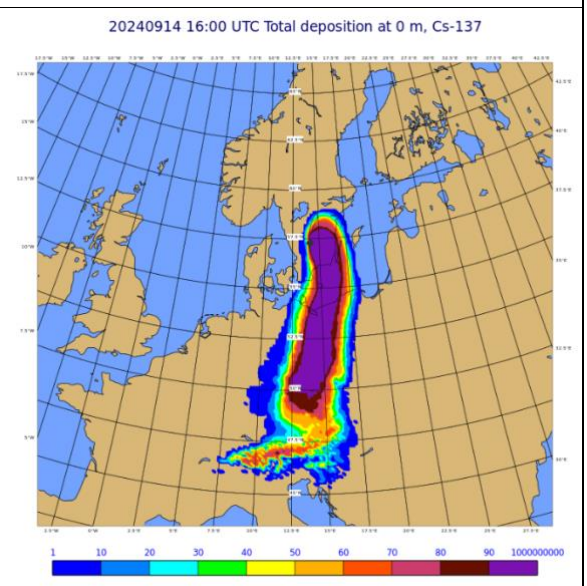  |

**Figure 16** Probability of exceeding a total accumulated ground deposited activity of $1 \cdot 10^4$ pBq/m$^2$ or Bq/m$^2$ at the end of simulation following either simulated detonation of a 100 kt nuclear device (NW) or simulated nuclear power plant accident (NPP) at Hagshult Airbase (black diamond) on September 12, 2024 at 16.00 UTC.

October 10, 2024, 08.00 UTC

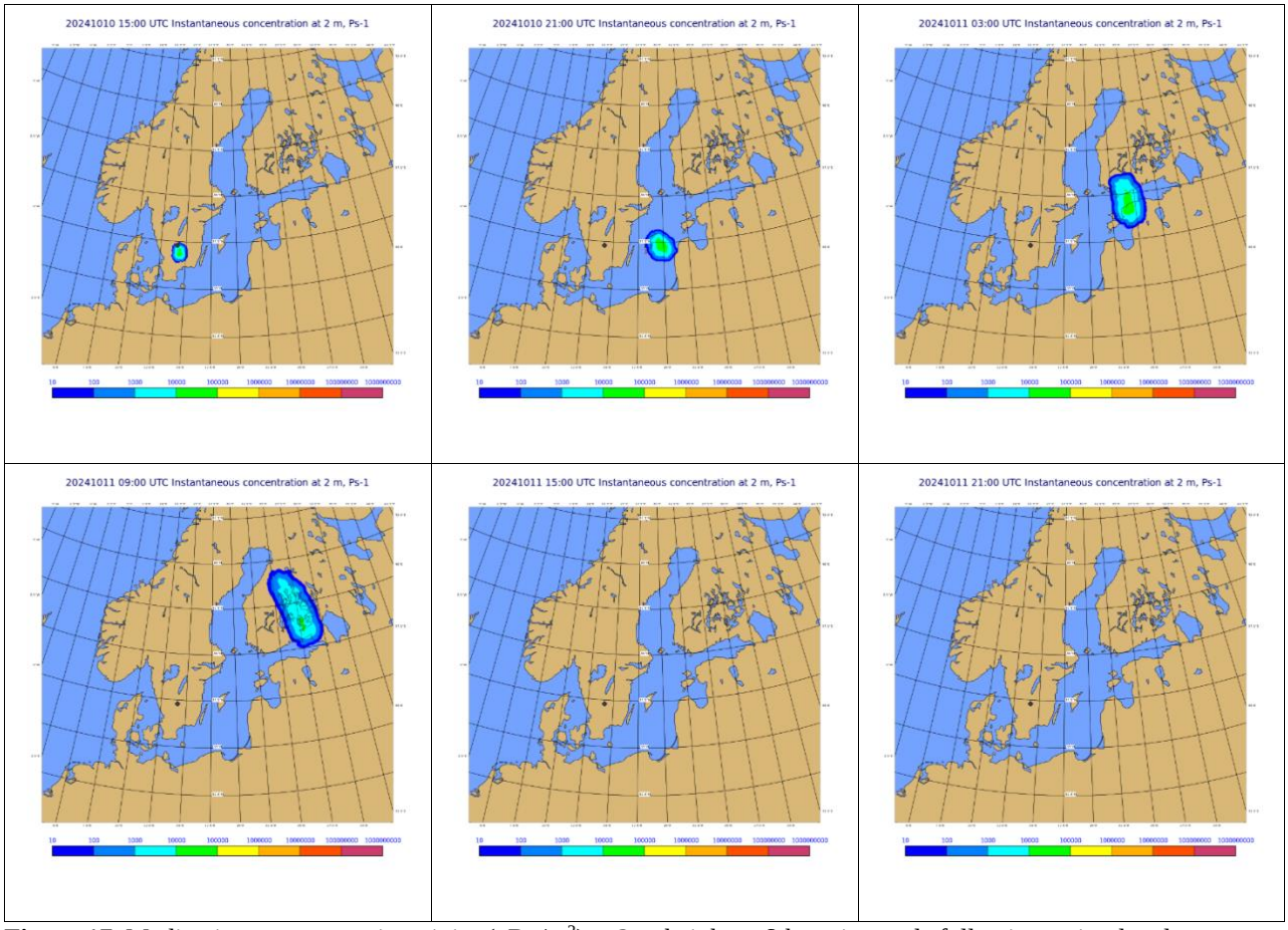


**Figure 17** Median instantaneous air activity (pBq/m$^3$) at 2 m height at 6-hour intervals following a simulated detonation of a 100 kt nuclear device at Hagshult Airbase (black diamond) on October 10, 2024 at 08.00 UTC.

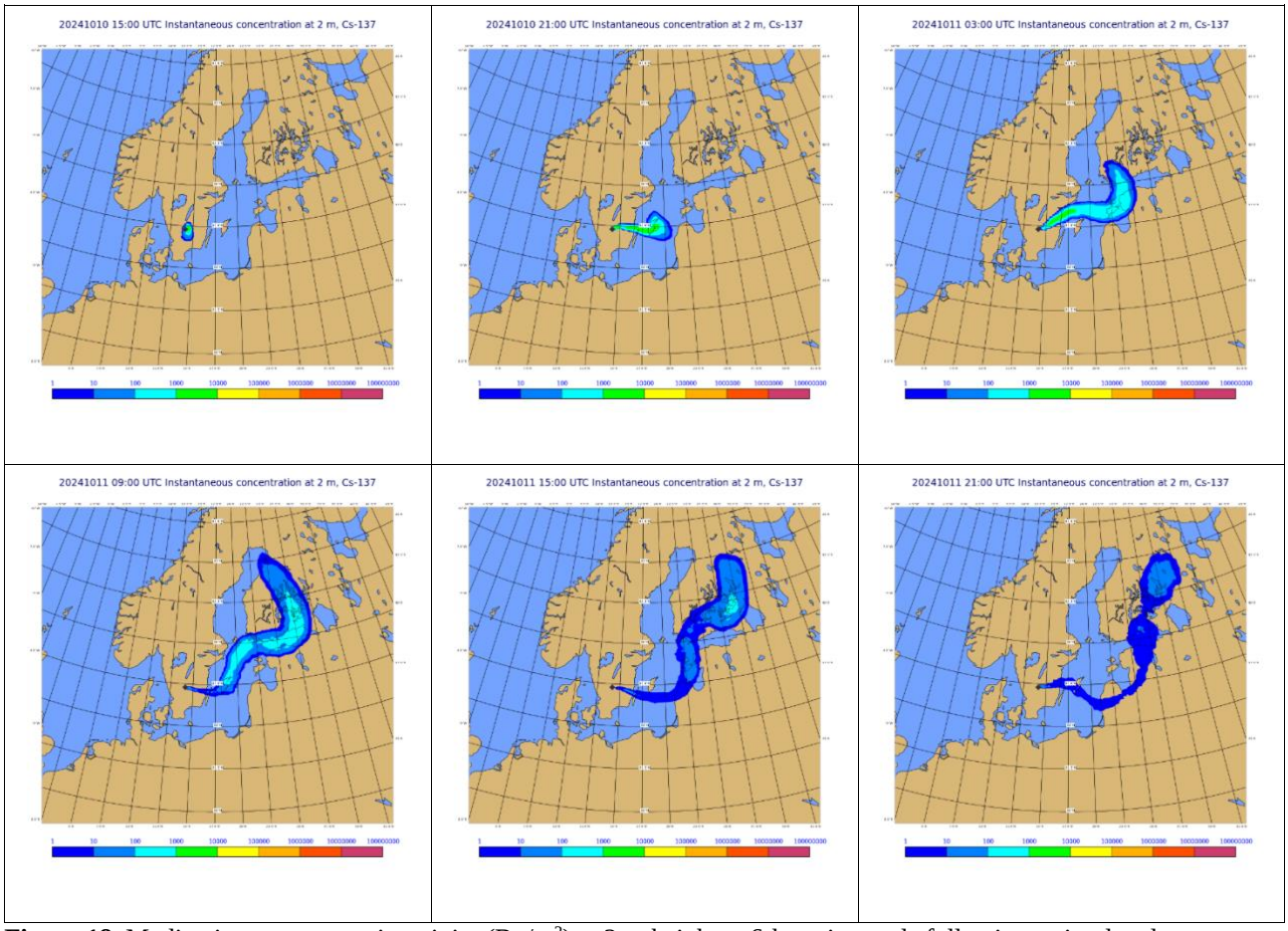


**Figure 18** Median instantaneous air activity (Bq/m$^3$) at 2 m height at 6-hour intervals following a simulated accident at a hypthetical nuclear power plant at the location of the Hagshult Airbase (black diamond) starting on October 10, 2024 at 08.00 UTC.

| Emission | 10th percentile | 50th percentile | 90th percentile |
|---|---|---|---|
| NW | 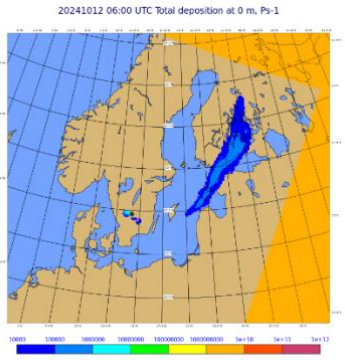 | 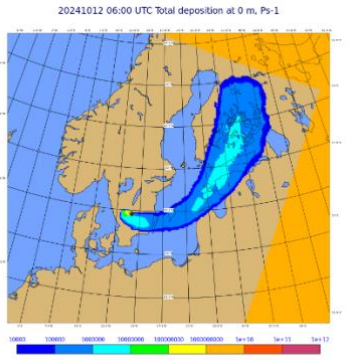 | 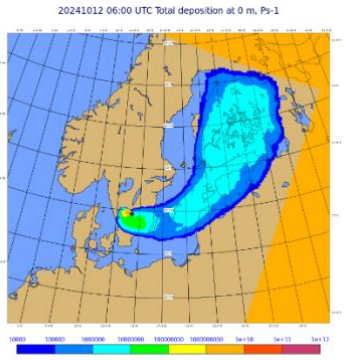 |
| NPP | 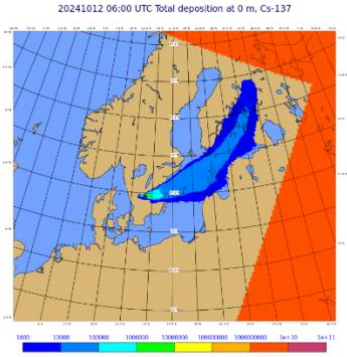 | 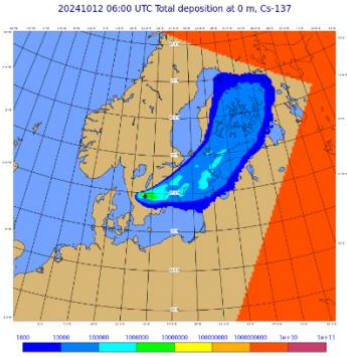 | 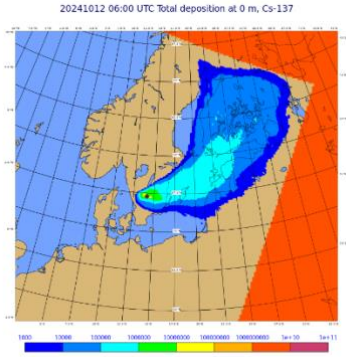 |

**Figure 19** 10th, 50th and 90th percentile of total accumulated ground deposited activity (pBq/m$^2$ or Bq/m$^2$) at the end of simulation following either simulated detonation of a 100 kt nuclear device (NW) or simulated nuclear power plant accident (NPP) at Hagshult Airbase (black diamond) on October 10, 2024 at 08.00 UTC. The colored box surrounding the figures show the outline of the NWP domain.

| Emission | 10th percentile | 50th percentile | 90th percentile |
|---|---|---|---|
| NW | 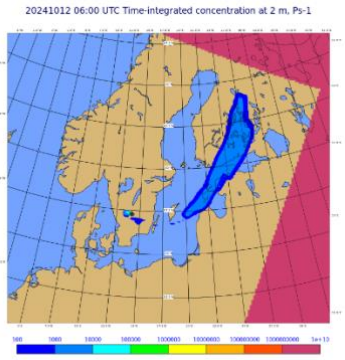 | 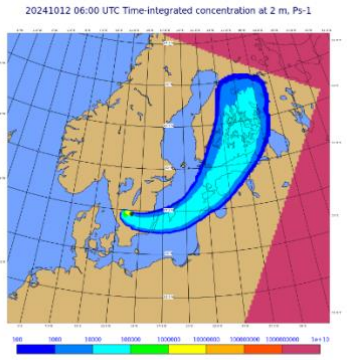 | 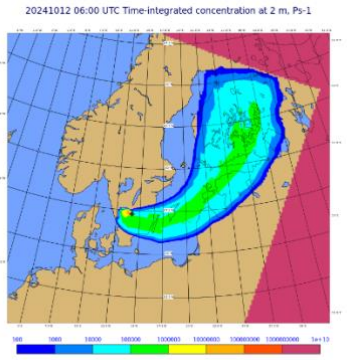 |
| NPP | 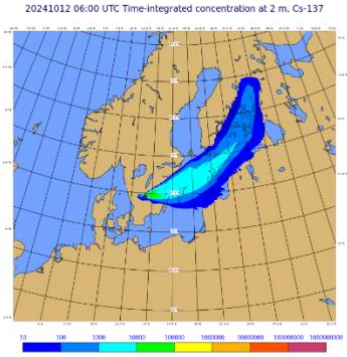 | 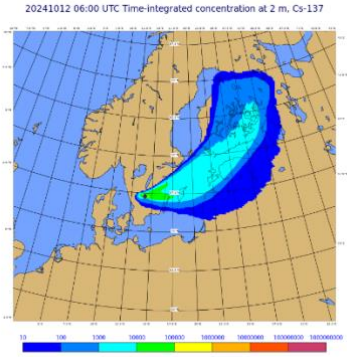 | 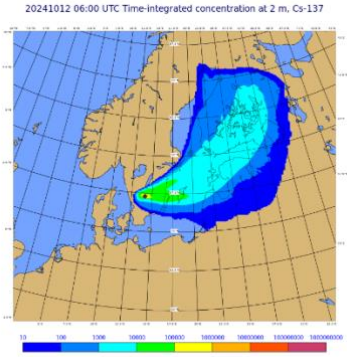 |

**Figure 20** 10th, 50th and 90th percentile of time-integrated air activity (pBq h/m$^3$ or Bq h/m$^3$) at 2 m height at the end of simulation following either simulated detonation of a 100 kt nuclear device (NW) or simulated nuclear power plant accident (NPP) at Hagshult Airbase (black diamond) on October 10, 2024 at 08.00 UTC. The colored box surrounding the figures show the outline of the NWP domain.

| NW | NPP |
| --- | --- |
| 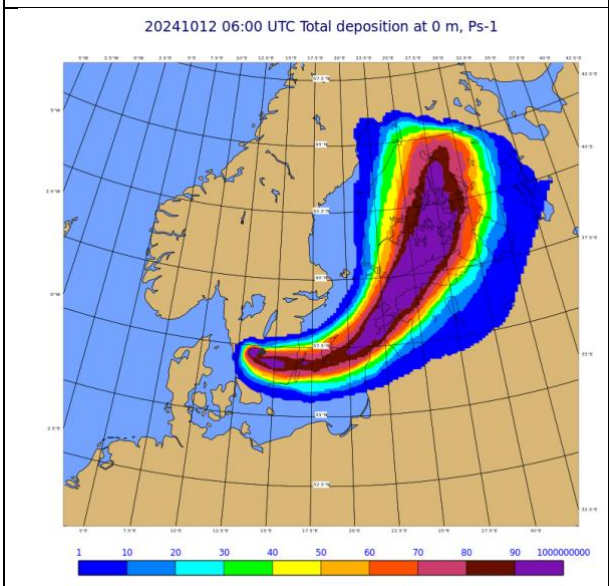  | 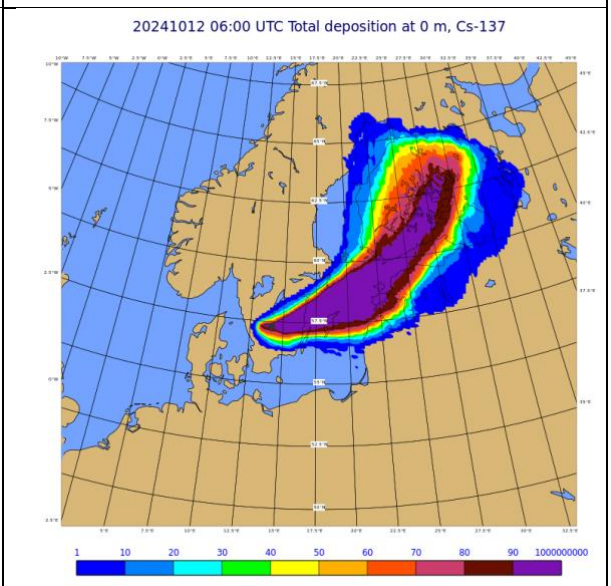  |

**Figure 21** Probability of exceeding a total accumulated ground deposited activity of $1{\cdot}10^4$ pBq/m$^2$ or Bq/m$^2$ at the end of simulation following either simulated detonation of a 100 kt nuclear device (NW) or simulated nuclear power plant accident (NPP) at Hagshult Airbase (black diamond) on October 10, 2024 at 08.00 UTC.

October 24, 2024, 16.00 UTC

| Emission | 10th percentile | 50th percentile | 90th percentile |
|---|---|---|---|
| NW | 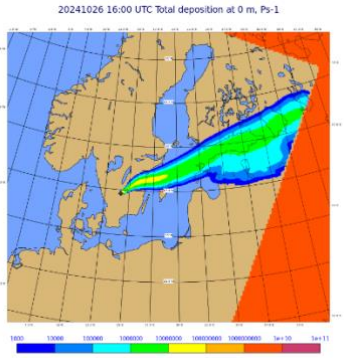  | 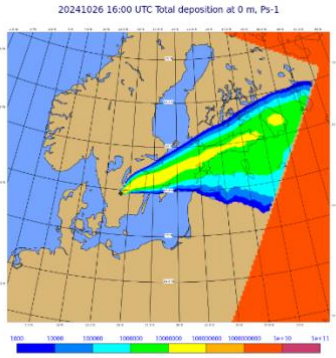  | 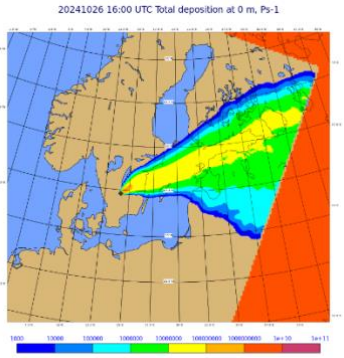  |
| NPP | 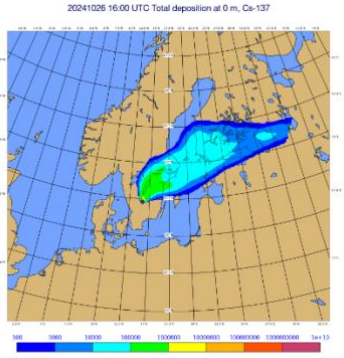  | 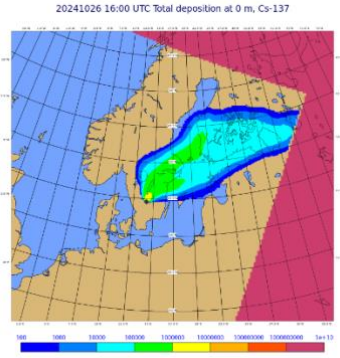  | 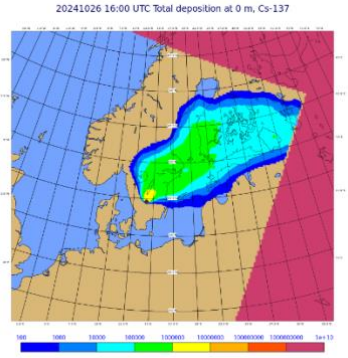  |

**Figure 22** 10th, 50th and 90th percentile of total accumulated ground deposited activity (pBq/m$^2$ or Bq/m$^2$) at the end of simulation following either simulated detonation of a 100 kt nuclear device (NW) or simulated nuclear power plant accident (NPP) at Hagshult Airbase (black diamond) on October 24, 2024 at 16.00 UTC. The colored box surrounding the figures show the outline of the NWP domain.

| Emission | 10th percentile | 50th percentile | 90th percentile |
|---|---|---|---|
| NW | 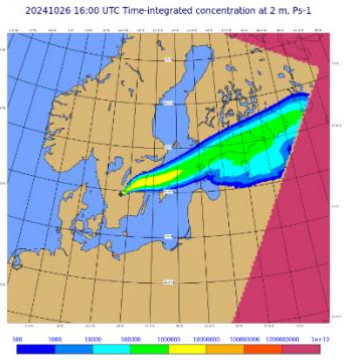  | 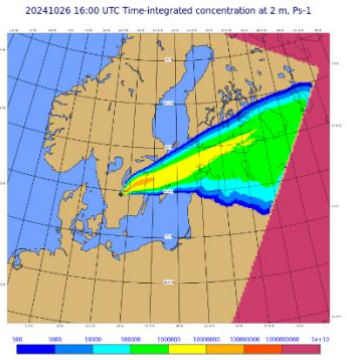  | 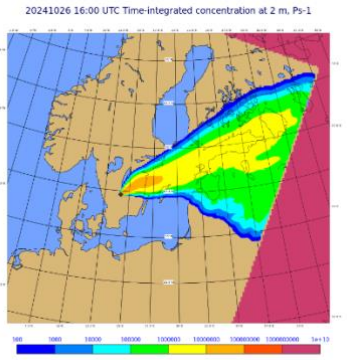  |
| NPP | 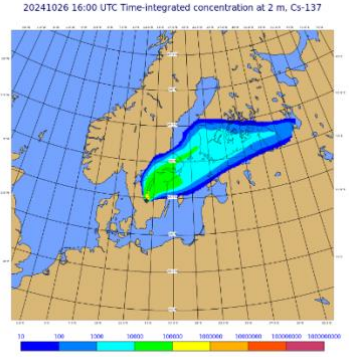  | 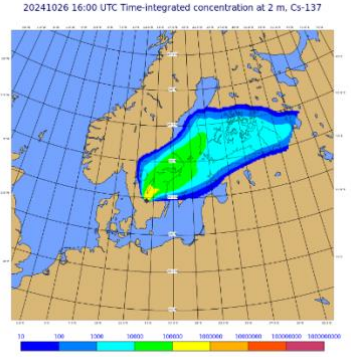  | 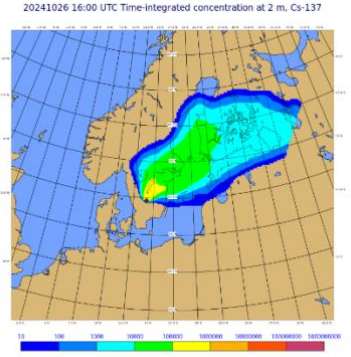  |

**Figure 23** 10th, 50th and 90th percentile of time-integrated air activity (pBq h/m$^3$ or Bq h/m$^3$) at 2 m height at the end of simulation following either simulated detonation of a 100 kt nuclear device (NW) or simulated nuclear power plant accident (NPP) at Hagshult Airbase (black diamond) on October 24, 2024 at 16.00 UTC. The colored box surrounding the figures show the outline of the NWP domain.

| NW | NPP |
| --- | --- |
| 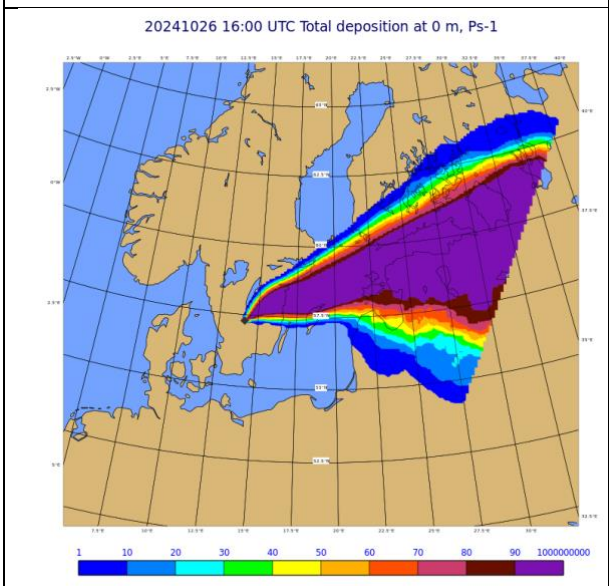  | 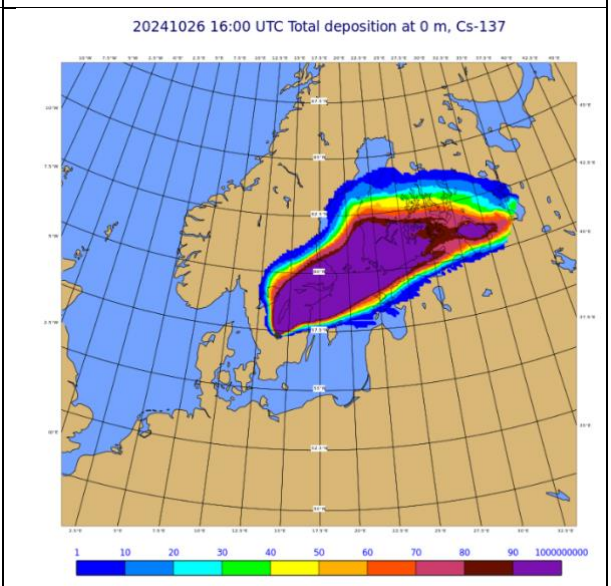  |

**Figure 24** Probability of exceeding a total accumulated ground deposited activity of $1 \cdot 10^4$ pBq/m$^2$ or Bq/m$^2$ at the end of simulation following either simulated detonation of a 100 kt nuclear device (NW) or simulated nuclear power plant accident (NPP) at Hagshult Airbase (black diamond) on October 24, 2024 at 16.00 UTC.

## *Discussion*

### Nuclear power plant accident

The meteorological uncertainty from accidental releases at nuclear power plants has previously been studied in the NKS-B projects MUD, FAUNA, MESO, and AVESOME, cf. Sørensen *et al.* (2014, 2016, 2017, and 2019). These studies employed methods similar to those used here, but with results based on different NWP ensembles and meteorological cases. Unsurprisingly, we find that the case-dependent meteorological uncertainty for the nuclear power plant accidents found here are comparable to those observed previously, as seen in Figure 15–17 and Figure 20–22. Overall, the difference between the 10$^{th}$ and 90$^{th}$ percentile deposition and time-integrated activities at a given location is typically about an order of magnitude. Correspondingly, the total geographical extent of the modelled activities is significantly larger for the 90$^{th}$ percentile. Comparable variation is observed for the deposition and time-integrated concentration at 2 m, as can be expected since they are calculated from the same dispersion modelling.

### Nuclear weapon detonation

Given the novelty of our nuclear weapon modelling implementation, the meteorological uncertainty in the dispersion following a nuclear detonation has not been studied in the previous NKS-B projects described above. The overall inter-percentile variation for the deposition and time-integrated activities for the nuclear weapon detonation is comparable to that of the nuclear power plant accident (Figure 15–17 and Figure 20–22). This is somewhat surprising given the very different emission durations (1 minute versus 48 hours), as one

might expect that the burst-like emission following the nuclear detonation would render it more sensitive to the exact meteorological conditions at the time of emission.

This seems to be the effect observed for the October 10 case with the most severe weather, as the results for the nuclear weapon dispersion modelling do seem to have somewhat larger uncertainty compared to the comparable case for the nuclear power plant accident. This highlights the case-sensitivity of the overall meteorological uncertainty on the dispersion, and thus the importance of modelling for the specific scenarios.

### Comparison

A direct comparison of the deposition and time-integrated activities following the modelled nuclear detonation and nuclear power plant accident has little meaning given the vastly different activity released overall, and the use of pseudo-nuclides for the nuclear-weapon simulations. However, surprisingly, the geographical extent of the dispersion is comparable in the two cases despite the vastly different emission scenarios (Figure 15–17 and Figure 20–22). However, as can be seen from Figures 18 and 19, the mechanism leading to the comparable deposition and time-integrated concentration patterns is quite different for the two cases reflecting the difference in emission duration. For the nuclear weapon detonation modelling, a short cloud of radiation is emitted and is advected, affecting the environment (Figure 18). However, as seen in Figure 14, the majority of the total activity from the detonation is located many kilometers above the surface and for some of the simulations, the instantaneous surface activity is replenished by activity descending from above.

In contrast, given the continued release from the nuclear power plant, also the airborne activity is continuous leading to gradual build-up of deposition and time-integrated concentration. Thus e.g. for periods of lower wind speeds or more variable wind directions, one might expect larger geographical areas to be affected by the nuclear power plant accident.

## Multi-scale Atmospheric Transport and Chemistry model (MATCH)

The Multi-scale Atmospheric Transport and Chemistry model (MATCH) (Robertson *et al.*, 1999) is multi-purpose Eulerian chemical transport model (CTM) developed by the SMHI. The model is used for emergency applications such as nuclear and natural events (volcanoes), aerosol dynamics and optics (Andersson *et al.*, 2015), complex chemistry, and data assimilation (Robertson and Langner, 1998; Kahnert, 2008; Kahnert, 2018). The MATCH model is used operationally for chemical forecasts in CAMS (Copernicus Atmospheric Monitoring Service) and for SSM (Swedish Radiation Safety Authority) serving the ARGOS system needs (Hoe *et al.*, 1999; 2002). Other applications are studies for air quality and health issues in climate projections. In most applications MATCH is used as a limited-area model on various possible scales, but also for global applications.

The MATCH model is basically an Eulerian model, but for emergency preparedness and response applications a Lagrangian particle model is used in the near field of the emission location.

A wide range of possible driving meteorological data is applicable like analyses and forecasts from HARMONIE, IFS (Integrated Forecasting System) developed and run by ECMWF (European Centre for Medium-Range Weather Forecasts), and WRF (Weather Research and Forecasting).

For nuclear weapon simulations, the operational MATCH model is initialised based on KDFOC3 (Harvey *et al.*, 1992) with procedures developed at FOI. The procedures handle underground detonations, as well as upper air detonation with or without surface contact (Winter *et al*, 2008).

### Dynamic description of nuclear initial clouds

This contribution intended to take advantage of dynamic description of the initial cloud development through the paper of Arthur *et al.* (2021) describing an implementation of a fireball evolution inside the WRF model. The paper defines an initial fireball which extent is described as spherical volume enclosing an energy of 1/3 of the yield for a prescribed heat excess Δθ at the centre. The fireball is described as the following:

$$\theta = \theta_{bg} + \frac{\Delta\theta}{2}\left[cos(\frac{\pi r}{R}) + 1)\right]$$

$$\Delta E = cp\Delta TM$$

$$\Delta TM = \int_V (\theta - \theta_{bg})\left(\frac{p}{p_0}\right)^{r_d/cp} \frac{p}{r_d\theta\left(\frac{p}{p_0}\right)^{r_d/cp}} dV$$

$$\Delta E \approx Y/3 \text{ (in Joules)}$$

The conversion from yield in kT TNT to Joules goes by the factor $4.184 \times 10^{12}$. The fireball is of the order of 100-600 m that implies rather fine resolution of the grid to represent the initial cloud. We have adopted a grid with a resolution of 50 m that is an interpolation using HARMONIE meteorological data at 2.5 km resolution. **Error! Reference source not found.** shows that our implementation arrive at radii comparable to Arthur *et al.* (2021).

**Table 3**. Evaluation of our implementation vs the ones given in the Arthur *et al.* (2021) for three of the Los Alamos nuclear tests.

| Event | Yield (kt) | Arthur et al. (2021) (m) | Our approach (m) |
|---|---|---|---|
| Dixie | 11 | 375 | 365 |
| Encore | 27 | 475 | 490 |
| Wasp | 1 | 155 | 171 |

In order to model the evolution of the fireball we have implemented a vorticity advection model following Murray (1970) described by the equation,

$$\frac{\partial \omega}{\partial t} = -\mathbf{v}\nabla\omega + \frac{\partial}{\partial x}\frac{\theta - \theta_{bg}}{\theta_{bg}} + \nu\nabla^2\omega$$

where the normalised heat excess $(\theta - \theta_{bg})/\theta_{bg}$ contributes to the vorticity by its lateral gradient, and the vorticity is defined by,

$$\underline{\omega} = \nabla \times \mathbf{v}$$

The advective wind is found by assuming the wind being the curl of a vector potential, $\psi$,

$$\mathbf{v} = \nabla \times \psi$$

and we will then arrive at a Poisson equation,

$$\omega = \nabla \times \nabla \times \psi = \nabla^2\psi$$

Solving the Poisson equation driven by the current vorticity we derive the wind, by the curl of the vector potential, needed in the advection. This forms the set of equations progressing the vorticity and the advection of potential temperature, humidity, liquid water and a virtual activity cloud.

A thorough description is found in Appendix A. Figure 25 illustrates the mayor elements of the vorticity equation at the starting point. In Figure 27 and Figure 28 the evolution of the fireball and liquid water are shown. Conferring to the stabilised cloud by KDFOC3 in Figure 28 the horizontal extension from the modelling is of the order of KDFOC3 while the vertical rise to 10 km is lower than described by KDFOC3 that is about 14 km. This model needs 45 minutes to reach a stabilised cloud while the modelling in Arthur *et al.* (2021) is about 15 minutes.

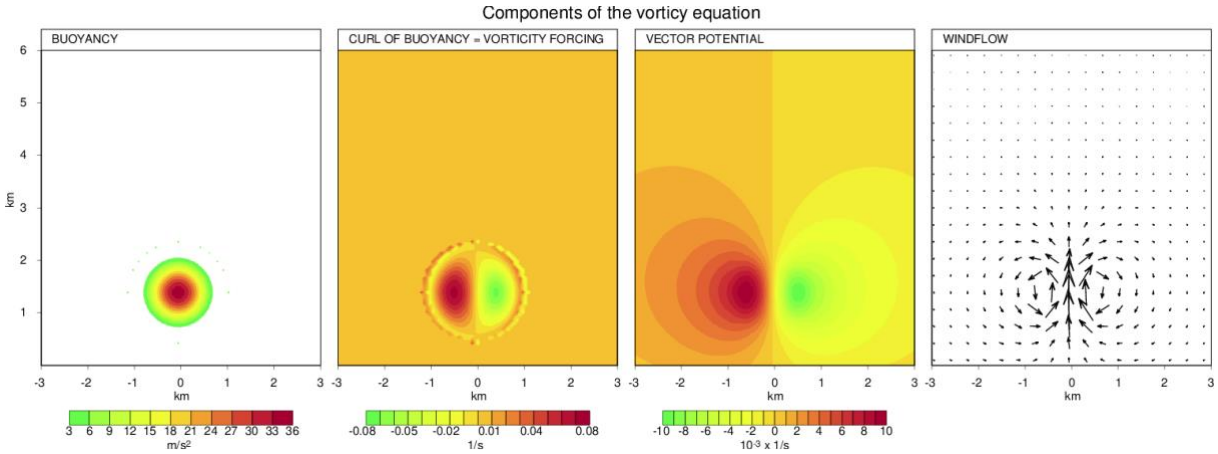


**Figure 25** The vorticity equation components; buoyancy (left), lateral gradient of buoyancy, vorticity (second), velocity potential (third) and resulting winds (right). The transformation of the buoyancy term (left panel) in polar coordinates into the Cartesian grid provide a numerical challenge that explains the a bit noisy pattern in the second panel.

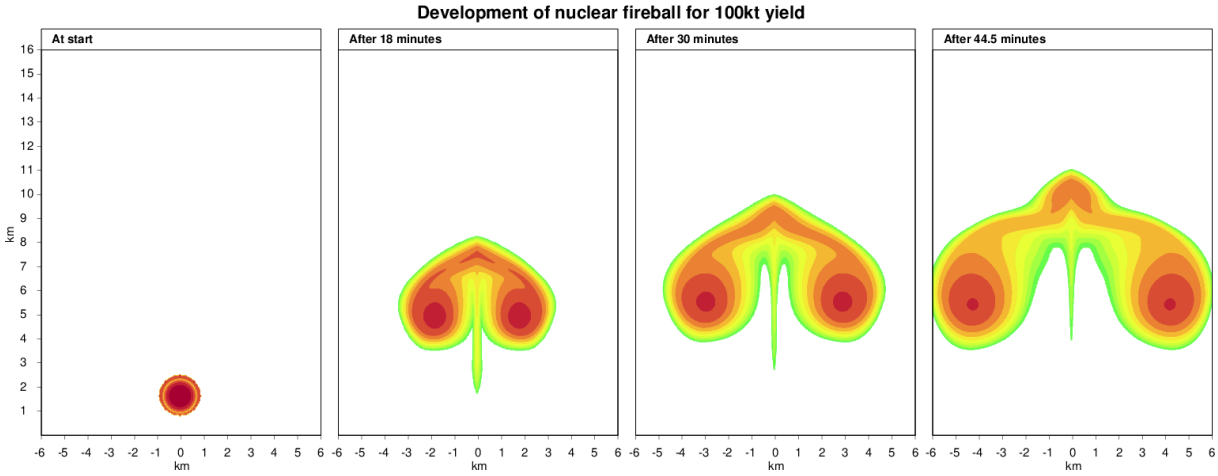


**Figure 26** A sequence of the evolution of the fireball at start (left), after modelled 10 minutes (second), after 30 minutes (third) and after 45 minutes (right). The colour shading could be interpreted as different level of activity concentrations.

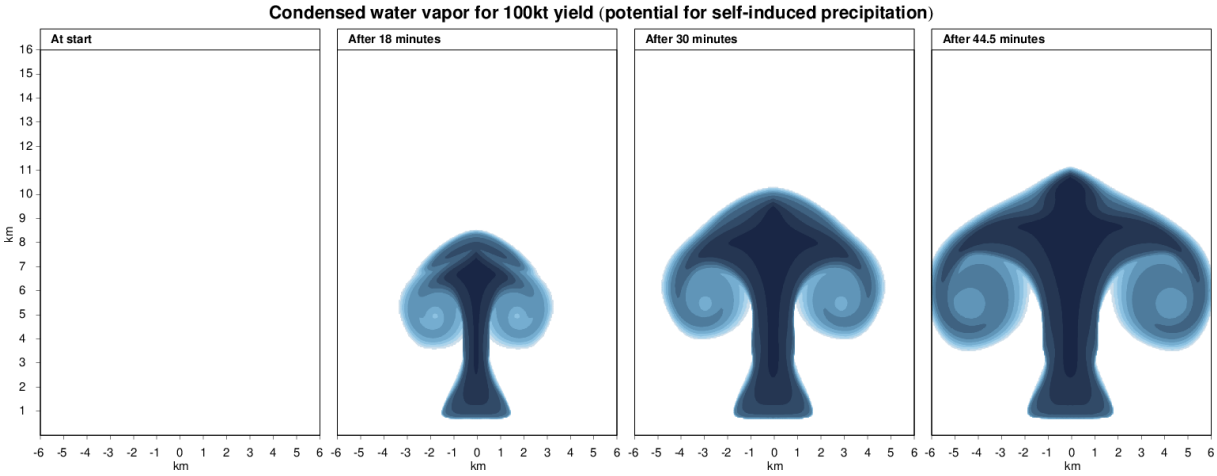


**Figure 27** A sequence of the evolution of induced liquid water at start (left), after modelled 10 minutes (second), after 30 minutes (third) and after 45 minutes (right). The induced liquid water is the prerequisite for self-induced precipitation.

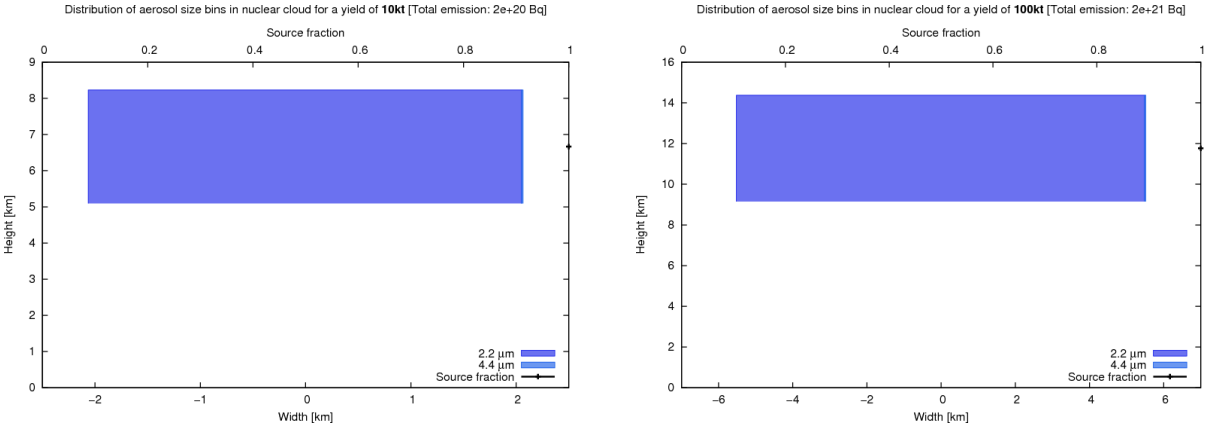


**Figure 28** Stabilised cloud based on KDFOC3 for 10 kt yield (left) and 100 kt yield (right).

## *Summary*

We have rather successfully managed to explore the article by Arthur *et al.* (2021) for separate modelling of the fireball from a vorticity transport model perspective. The width of the stabilised cloud arrives in the order described by KDFOC3 but the rise level does not reach the same level as described in KDFOC3. We notice though that our modelling gives a slower rise than shown in Arthur *et al.* (2021) with 45 minutes in our case in comparison to about 15 minutes in Arthur *et al.* (2021). Moreover, our simulations use about 1 hour of simulations having time-steps ~1 second. From an operational point of view we may not foresee any practical use, but we may further look into self-induces precipitation that could be tabulated for operational applications.

### *Application to Selected Cases*

HARMONIE data are routinely archived on tape at SMHI. The full model volume is unfortunately not stored, only layers up to 4.5 km. A test for a June case is shown in Figure 30 and two cases for the storm Hans in Figure 31 and Figure 32 are therefore made for a 1 kt yield for which the extension and aerosol distribution is shown in Figure 29.

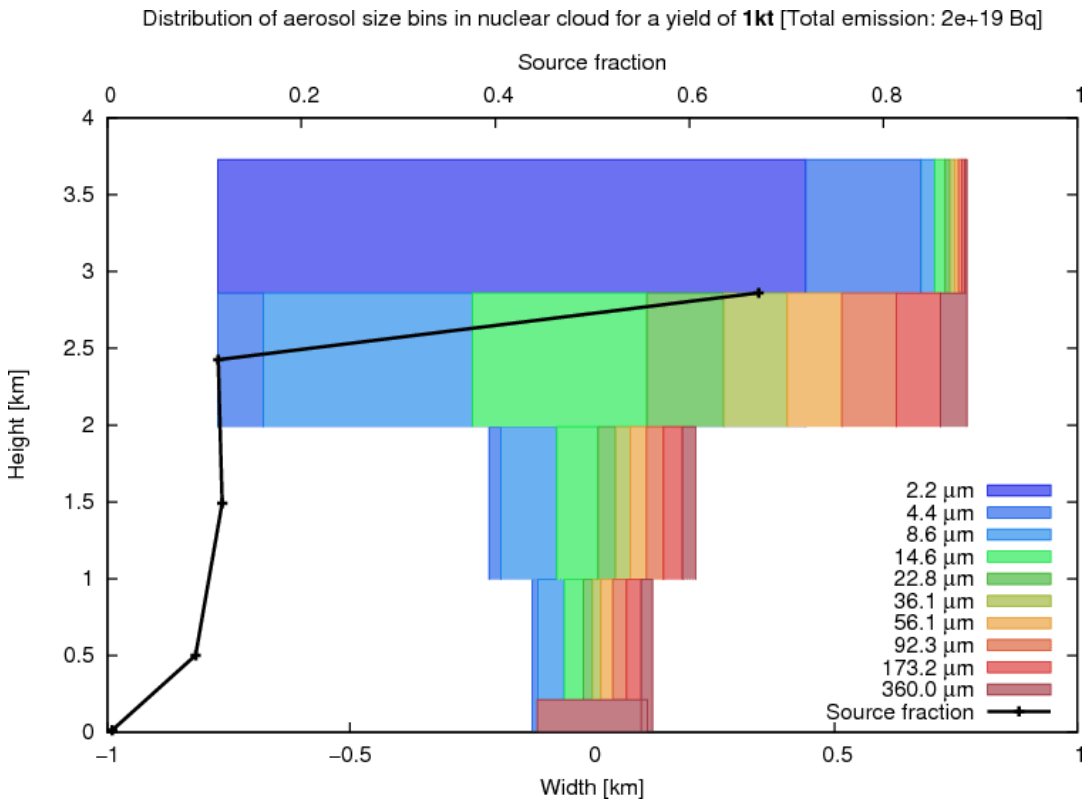


**Figure 29** KDFOC3 implementation for a 1 kt yield. The figure shows the extent and distribution of aerosol bins. The segments should be viewed as different cylinders forming the cloud. The black line shows the relative distribution of different parts of the cloud (scale at top of the panel). The top cylinder has two different distribution, one arising from the devise (top layer) and a second by the dust updraft (bottom layer).

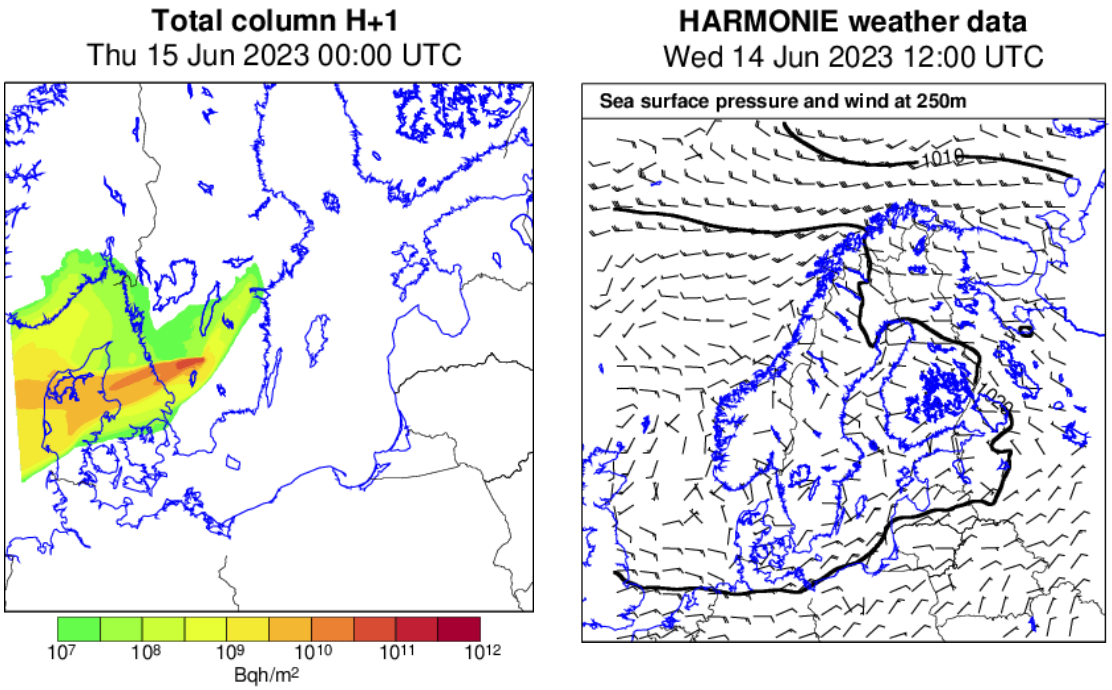


**Figure 30** Accumulated total column for a June case 2023 for a 1 kT device at Hagshult Airbase run for 13 June (00 UTC) to 15 June (00 UTC) and the weather chart for 14 June (12 UTC).

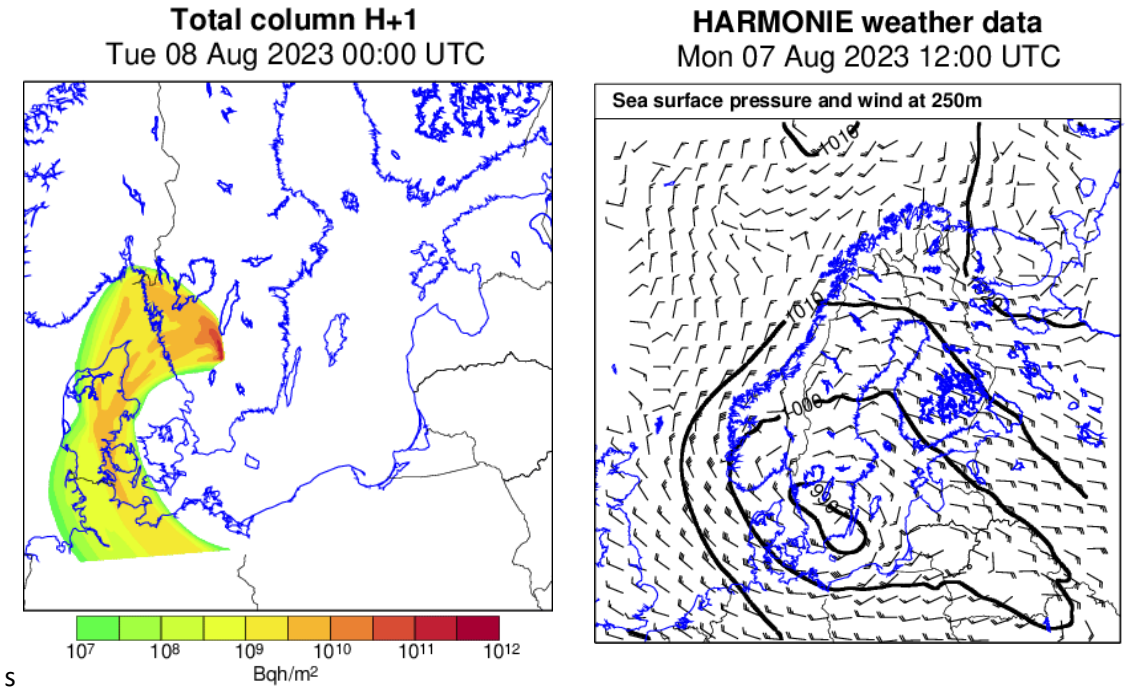


s

**Figure 31** Accumulated total column for the storm Hans case for a 1 kT device at Hagshult Airbase run for 6 August (00 UTC) to 8 August (00 UTC) and the weather chart for 7 August (12 UTC).

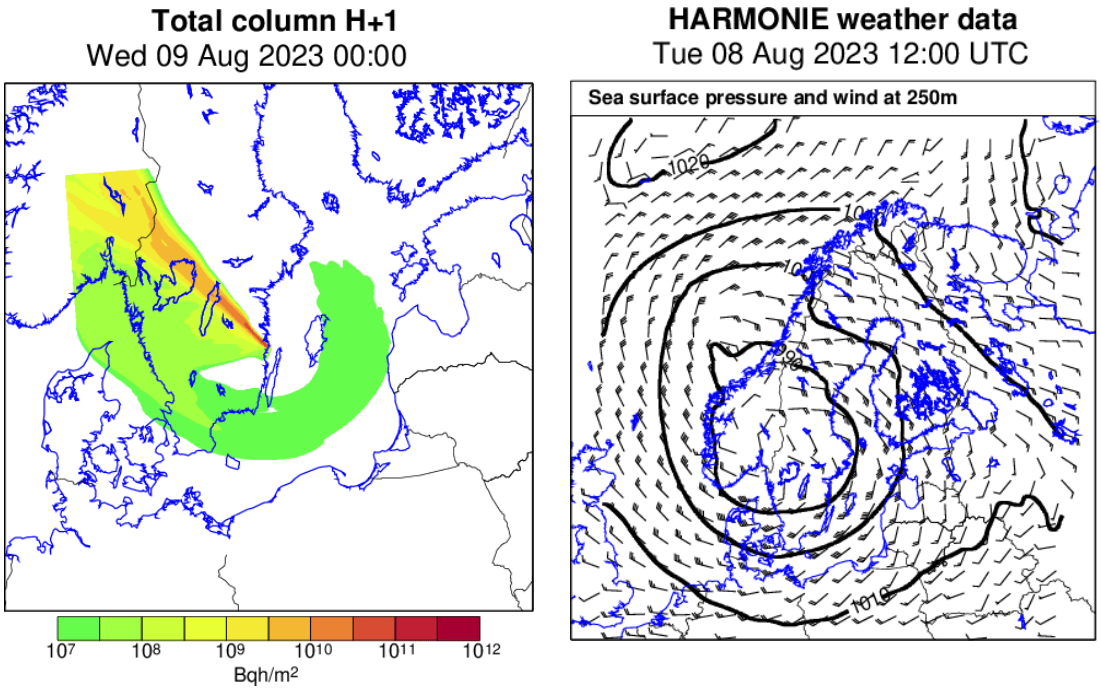


**Figure 32** Accumulated total column for the storm Hans case for a 1 kT device at Hagshult Airbase run for 7 August (00 UTC) to 9 August (00 UTC) and the weather chart for 8 August (12 UTC).

## NWSWAMP

NWSWAMP is a model that simulates the initial distribution of activity in a radioactive cloud after a nuclear burst and it is developed by the Swedish Defence Research Agency (FOI). The NWSWAMP model is an adaptation of KDFOC3 (Harvey *et al.*, 1992) for use together with Lagrangian particle models. NWSWAMP is used in combination with the random displacement particle model PELLO (Lindqvist, 1999) for long range dispersion simulations. NWSWAMP can also be used as a standalone library, which is implemented at SMHI for use in the Eulerian dispersion model MATCH-BOMB (Robertson *et al.*, 1999) on behalf of SSM for nuclear and radiological emergency response.

KDFOC3 is a "disc tosser" model where the radioactivity is distributed into a number of discs of different sizes distributed in height. The horizontal discs are distributed over a stabilized cloud modelled as two or three cylindrically symmetric parts, with a common vertical axis of symmetry. For surface and low air bursts there are two disjoint parts, a *stem cloud* shaped as a right frustum of a circular cone, with the smaller base attached to the ground, and on top of the stem cloud attached a *main cloud* shaped as a circular cylinder. For shallow and deep bursts there is an additional *base surge cloud*, shaped as a vertical cylinder attached to the ground. For shallow bursts, the base surge cloud overlaps the lower part of the stem cloud, whereas for deep bursts, the base surge cloud overlaps the entire stem cloud and part of the main cloud. See Harvey *et al.* (1992), Figure 2.3.2 for graphical illustrations. The dimensions of the stem, main and base surge clouds are parametrized continuously in terms of the total yield and the height of burst ($hob$) / depth of burial ($dob$). The activity size distribution in the

stabilized cloud is modeled by a mixture of two lognormal distributions, or modes, of particles, one “large” and one “small”. The parameters of the distributions are fixed for deep buried bursts and surface or low air bursts. For shallow buried bursts, the parameters are determined by linear interpolation with the scaled depth of burial

$$sdob = 3.281 \times dob \times wtot^{-0.294}$$

cf. Harvey et al. (1992), p. 47-48. The mode descriptions come from empirical studies that preceded KDFOC3 but can be interpreted as a surface mode and a volume mode represented by “large” and “small”.

In the dataset used for the KDFOC3 model descriptions there were two modes visible which support the approach, but the KDFOC report Harvey *et al.* (1992)does not go into detail of what constitutes these two modes.

For each mode in the mixture, a piecewise linear altitude distribution is used. The construction of this is elaborated on below. The radial distribution at a fixed level is assumed Gaussian with standard deviation equal to the cloud radius at that level, for both modes.

For air bursts ($hob > 0$), a volume fraction

$$fhob = \left(1 + \frac{hob}{2rb}\right) \times \left(1 - \frac{hob}{rb}\right)^2$$

is used, were the free air-burst radius $rb$ is defined by

$$rb = 55 wtot^{0.4} [m]$$

see Figure 33.

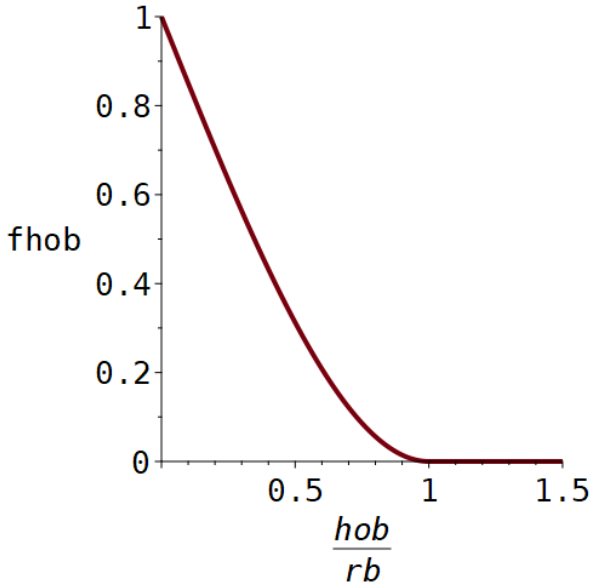


**Figure 33** Volume fraction used for air bursts (hob>0).

The ground zero circle is represented with five shallow cylinders with model particles that directly deposits due to gravitational settling, since it represents very large particles. When there is a detonation below the surface a base surge cloud is created. This is also divided in a top and a bottom cloud with a large and a small mode of particles in each.

In the NWSWAMP model the source for *global fallout* is always located at the main cloud (nothing is located in the stem cloud). These particles are all the particles smaller than 5 $\mu$m coming both from surface debris or evaporated bomb material. In the case of the high altitude burst, all radioactive particles are represented as global fallout.

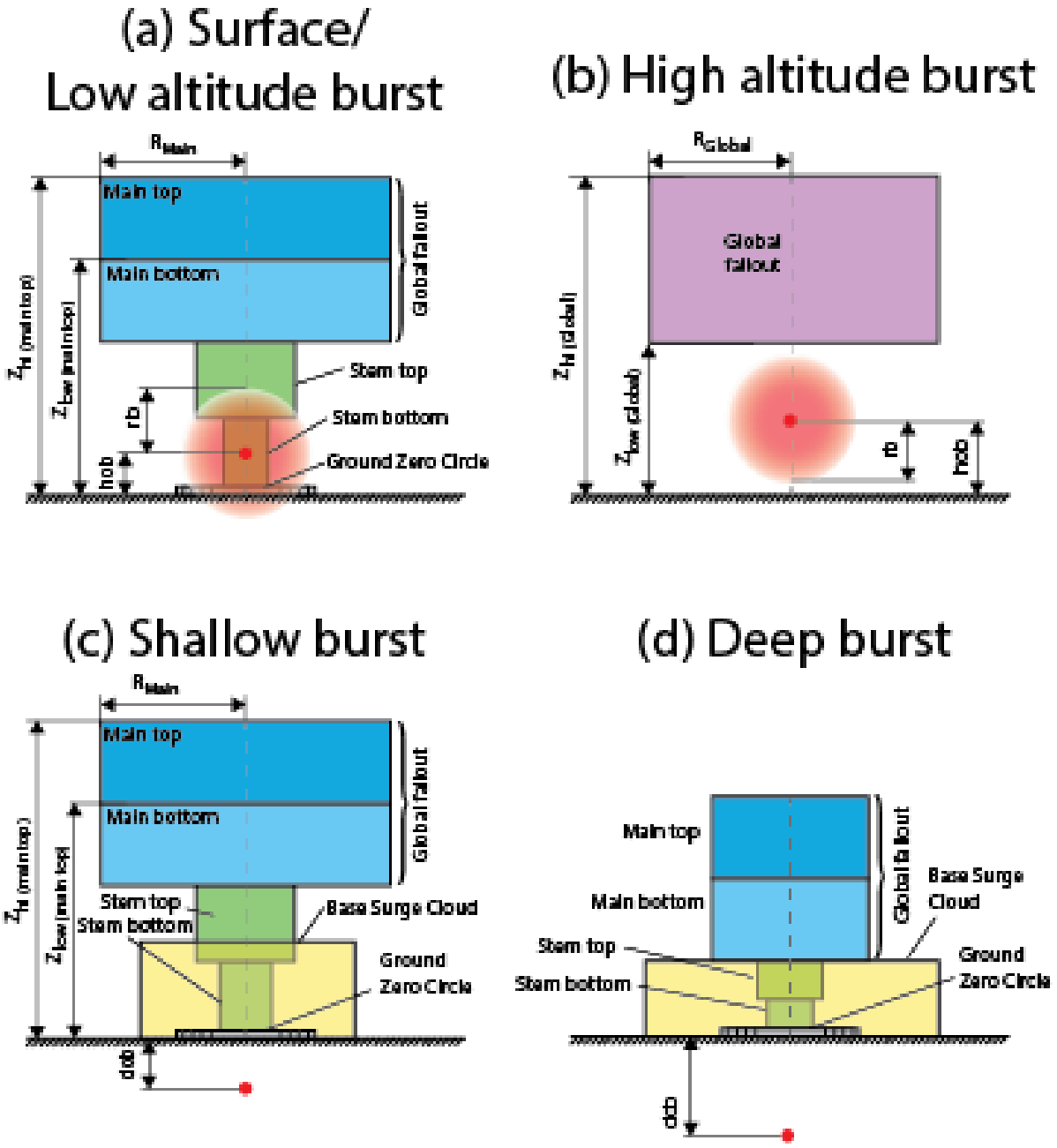


**Figure 34** Visualisation of the different sub-sources that are output from NWSWAMP: Main cloud top, Main cloud bottom, Stem cloud top, Stem cloud Bottom, Global fallout, Ground zero circle (5 sub-sources with different radius) and Base surge cloud (only for buried bursts). Each sub-source has dimensions set by the variables $Z_{hi}$, $Z_{lo}$ and R (visualized only for main cloud top in (a) and Global fallout in (b)). The location of the burst is visualised with the centre of the fireball and is in these figures visualized as *hob*, height of burst, or *dob*, depth of burial. In the code, and while using the library, *dob* is used both for buried burst and for altitude bursts with a negative sign. This nomenclature comes from the original KDFOC3 description.

KDFOC3 is constructed to calculate the fallout of radioactive debris in the vicinity of the detonation. Particles smaller than 5 $\mu$m in radius is therefore neglected in KDFOC3 but have been added in NWSWAMP to better represent regional and global dispersion scenarios. The smaller part of the spectrum is added by assuming that the radioactivity omitted in KDFOC3 (compared to the total radioactivity released in the detonation) preferably will stick to the

surface of particles smaller than 5 $\mu$m in radius, thus linking the smallest particles to one of the already existing particle distributions used in the model. The details for this procedure are presented in a FOI-report (Winter *et al.*, 2008), in Swedish, and is here added below for the convenience for the readers.

The following section (with font Arial) is translated from Winter *et al.* (2008):

> The activity on small particle radii (which is missing in KDFOC3) has been added in the form of a separate auxiliary source, located as the main cloud. For a surface explosion or air explosion, i.e. to *hob*[1] $\geq 0$, the new source will have the activity
>
> $$wac\_o = \max\left[0, wfe - wfa - wactot\_gz\right] \text{ for } hob \geq 0$$
>
> where *wfe* = the total generated activity, *wfa* = total airborne activity (at radii > 5 μm) according to the original KDFOC3 report, and *wactot_gz* = the activity on the ground zero circle. The activity of the new source thus complements the total activity *wfe*.
>
> For an underground explosion, parts of the total activity *wfe* will become trapped and remain in the ground substrate, so the simple complementary principle above cannot be applied. A study of the KDFOC3 model, however, shows that *wac_0* is connected to the so-called "vent fraction" (see Harvey *et al.* (1992)) in a certain way. For an underground explosion, i.e. the depth of burial = *dob* > 0, the new source will then have the activity
>
> $$wac\_0 = \max\left[0, wfe\left(1 - 0.7665 \cdot e^{sdob/106}\right) - wactot\_\_gz\right] \text{ for } dob>0,$$
>
> where $sdob = 3.281 \cdot dob \cdot wtot^{-0.294}$ .
>
> The distribution of activity on particle radii in the new source has been adapted to complement the truncated lognormal activity-size distributions found in the original KDFOC3 (for the larger particle radii). The lognormal activity radius distribution for the new source then has the following parameters:
>
> Median radius = *rbar_o* = (0.20 + 2.8 *fhob*) $\mu m$, geometric standard deviation = *sigma_o* = 2.75, lower cutoff = *rmin_o* = 0.01 $\mu m$, upper cutoff = *rmax_o* = 5.0 $\mu m$.
>
> *fhob* = 1 for *dob* > 0, *fhob* = 0 for *hob* > *rb* = $55 \cdot wtot^{0.4}$
>
> and
>
> $$fhob = \frac{(2rb + hob)(rb - hob)^2}{2rb^3} \text{ for } 0 \leq hob \leq rb.$$

A plot of the median radius as function of hob is found in Figure 35.

[1] *hob* - Height of burst

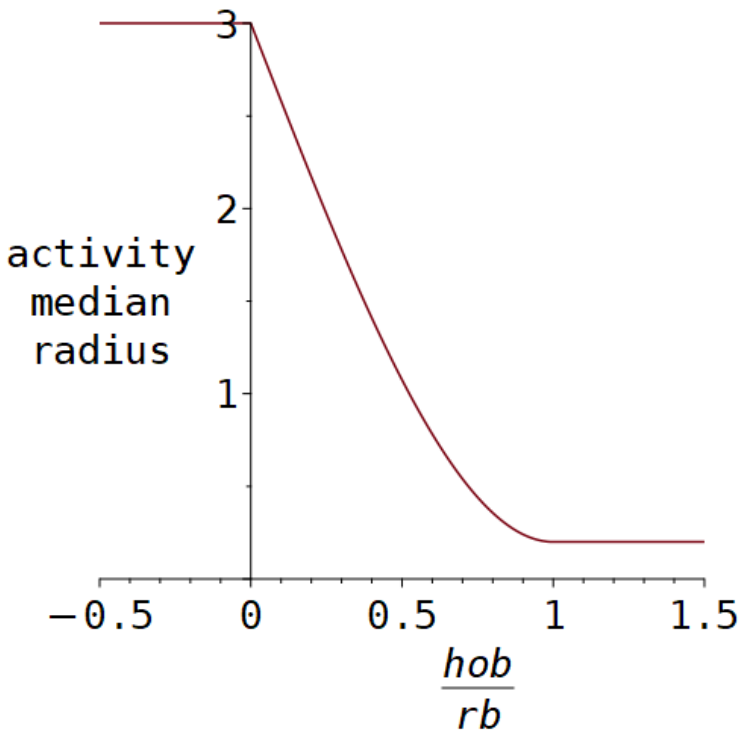


**Figure 35** The activity mean radius as function of hob/rb for the global fallout fraction.

The analysis performed by Baker (1987) suggests that the activity median radius of the small particle auxiliary source should be lowered to 0.10 $\mu$m. This does probably not affect the dispersion to a significant extent, since the settling velocity for such small particles is already very small. However, the deposition might be affected. This will be investigated in future work.

### The vertical activity distributions in KDFOC3

In this section we describe the construction of vertical activity distributions in KDFOC3.

To simplify formulas, we prefer to use a non-dimensional height coordinate $\zeta$, scaled such that $\zeta = 0$ at the ground, and $\zeta = 1$ at the top of the main cloud. The vertical distribution of activity is described in terms of triangular shape functions of the form

$$\varphi(\zeta) = \begin{cases} \hat{\varphi} \cdot (\zeta - \zeta_{min})/(\hat{\zeta} - \zeta_{min}), & \zeta_{min} \le \zeta \le \hat{\zeta} \\ \hat{\varphi} \cdot (1 - \zeta)/(1 - \hat{\zeta}), & \hat{\zeta} < \zeta \le 1 \end{cases}$$

where $0 < \hat{\zeta} < 1$ and $\zeta_{min} < 0$ are parameters, and the maximum value is

$$\hat{\varphi} = 2(\hat{\zeta} - \zeta_{min})/(\hat{\zeta} - \zeta_{min} - \hat{\zeta}\zeta_{min})$$

which yields

$$\int_0^1 \varphi(\zeta) d\zeta = 1.$$

To a shape function we also associate integrals (called area functions in [1])

$$I(\varphi,\zeta_b,\zeta_t)\equiv\int_{\zeta_b}^{\zeta_t}\varphi(\zeta)d\zeta=\begin{cases}\dfrac{\hat{\varphi}\cdot[(\zeta_t-\zeta_{min})^2-(\zeta_b-\zeta_{min})^2]}{2\left(\hat{\zeta}-\zeta_{min}\right)}, & \zeta_{min}\le\zeta_b<\zeta_t\le\hat{\zeta}\\ \dfrac{\hat{\varphi}\cdot[(1-\zeta_b)^2-(1-\zeta_t)^2]}{2\left(1-\hat{\zeta}\right)}, & \hat{\zeta}\le\zeta_b<\zeta_t\le 1\\ I\left(\varphi,\zeta_b,\hat{\zeta}\right)+I\left(\varphi,\hat{\zeta},\zeta_t\right), & \zeta_{min}\le\zeta_b<\hat{\zeta}<\zeta_t\le 1\end{cases}$$

and shape functions truncated to intervals $[\zeta_b,\zeta_t]$,

$$\varphi(\zeta;\zeta_b,\zeta_t)=\begin{cases}\varphi(\zeta), & \zeta_b\le\zeta\le\zeta_t\\ 0 & otherwise\end{cases}$$

Note that by the definitions above,

$$\int_0^1\varphi(\zeta;\zeta_b,\zeta_t)d\zeta=I(\varphi,\zeta_b,\zeta_t).$$

Given a collection of intervals $\left[\zeta_{b,n},\zeta_{t,n}\right], n=1,2,\ldots$, the functions $\psi_n(\zeta)=\varphi(\zeta;\zeta_{b,n},\zeta_{t,n})$ span a finite-dimensional space of functions

$$A(\zeta)=\sum\nolimits_n c_n\psi_n(\zeta).$$

In case $\psi_n(\zeta), n=1,2,\ldots$ are linearly independent, the coefficients $c_n$ are unique, and $\psi_n(\zeta)$ is a basis. If $\psi_n(\zeta), n=1,2,\ldots$ are linearly dependent, the coefficients $c_n$ are nonunique. However, $\psi_n(\zeta), n=1,2,\ldots$ constitutes a *frame*, and there is a unique coefficient vector with minimum norm, cf. Daubechies (1992), Proposition 3.2.4. The vertical activity distributions in KDFOC3 are of the form $A(\zeta)$ above.

More precisely, in KDOFC3 clouds are indexed by $n=1,2$ or $n=1,2,3$ if there is a base surge cloud, and particle modes are indexed by $k=1,2$. For each particle mode $k$ a shape function $\varphi_k(\zeta)$ and a frame $\psi_{k,n}(\zeta)=\varphi_k\left(\zeta;\zeta_{b,n},\zeta_{t,n}\right), n=1,2,\ldots$ is determined by choosing values of $\zeta_{min}$ and $\hat{\zeta}$. The default values used in KDFOC3 are $\zeta_{min}=-3/10$ for all $k$, and $\hat{\zeta}=2/3$ for $k=1$, $\hat{\zeta}=1/10$ for $k=2$. Moreover, $\zeta_{b,n}<\zeta_{t,n}$ denote the vertical limits for cloud $n$. The vertical activity distributions $A_k(\zeta)$ are determined by computing the coefficients $c_{k,n}$ in the representation

$$A_k(\zeta)=\sum\nolimits_n c_{k,n}\psi_{k,n}(\zeta).$$

The coefficients are computed as

$$c_{k,n}=A_{tot}u_k\,w_{k,n}/v_{k,n}$$

where

$$v_{k,n}=I\left(\psi_{k,n},0,1\right)=I\left(\varphi_k,\zeta_{b,n},\zeta_{t,n}\right),$$

and

$$w_{k,n} = u_{k,n}v_{k,n}/Z_k,$$

where

$$Z_k = \sum_n u_{k,n}v_{k,n},$$

cf. Harvey *et al.* (1992), p. 54 and the table below. Thus, $c_{k,n} = A_{tot}u_k\, u_{k,n}/Z_k$, and

$$A_k(\zeta) = \frac{A_{tot}u_k}{Z_k}\sum_n u_{k,n}\psi_{k,n}(\zeta).$$

Here,

$$u_k \geq 0, \sum_k u_k = 1,\ u_{k,n} \geq 0, \sum_k u_{k,n} = 1,\ n = 1,2,\ldots$$

The $u_k$ are weights for the distribution of the total airborne activity $A_{tot}$ onto the particle modes $= 1,2$ , and for each $k$, $u_{k,n}$ are weights for distribution of particle mode $k$ onto the clouds $n = 1,2,$ .... In KDFOC3, the vertical cloud limits $\zeta_{b,n}, \zeta_{t,n}$ and the weights $u_k, u_{k,n}$ are computed in terms of the scenario parameters.

***An example.***

Define $\varphi_k(\zeta)$ by choosing $\zeta_{min} = -3/10$ for all $k$, and choosing $\hat{\zeta} = 2/3$ for $k = 1$, $\hat{\zeta} = 1/10$ for $k = 2$, which is default in KDFOC3. Assume the particle mode weights $u_1 = 0.75, u_2 = 0.25$. Consider a stem cloud with $0 \leq \zeta \leq 1/3$ and a main cloud with $1/3 \leq \zeta \leq 1$, and assume the cloud weights

$$u_{1,1} = 0.3, u_{1,2} = 0.7, u_{2,1} = 0.9, u_{2,2} = 0.1.$$

Computing the "partition functions"

$$Z_1 = 0.593, Z_2 = 0.533$$

we get the following results in Figure 36:

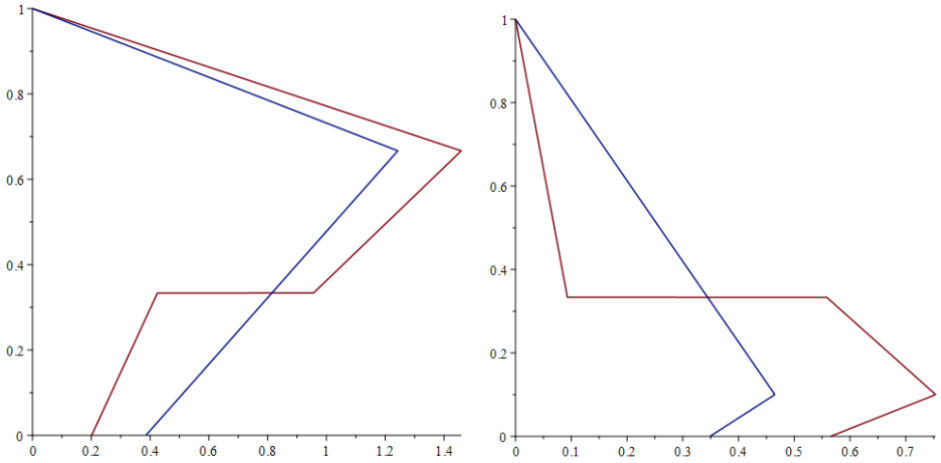

**Figure 36** Auxiliary distributions $\boldsymbol{u_k \varphi_k(\zeta)}$ (blue curves) and KDFOC3 distributions $\sum_n \boldsymbol{u_k\, u_{k,n} \psi_{k,n}(\zeta)/Z_k}$ (red curves), for $\boldsymbol{k = 1}$, small particles (left) and $\boldsymbol{k = 2}$, large particles (right).

The construction can be viewed as a redistribution of total activity in the auxiliary distributions, in such a way that the shape of the distributions within each cloud is preserved.

### *Modifications in NWSWAMP*

In NWSWAMP the frame functions $\psi_{k,n}$ are replaced by a piecewise constant approximation on a vertical bisection of the cloud, preserving the integral, viz.,

$$\tilde{\psi}_k(\zeta) = \begin{cases} I(\psi_k, \zeta_{b,n}, \zeta_{c,n})/I(\psi_k, \zeta_{b,n}, \zeta_{t,n}), & \zeta_{b,n} \le \zeta < \zeta_{c,n} \\ I(\psi_k, \zeta_{c,n}, \zeta_{t,n})/I(\psi_k, \zeta_{b,n}, \zeta_{t,n}), & \zeta_{c,n} \le \zeta < \zeta_{t,n} \\ 0 \quad otherwise \end{cases}$$

Here

$$\zeta_{c,n} = (\zeta_{b,n} + \zeta_{t,n})/2$$

is the bisection height. Similarly, the KDFOC3 affine radial function $r_n(\zeta), \zeta_{b,n} \le \zeta < \zeta_{t,n}$, defining the radial extent of cloud $n$, is replaced by a piecewise constant bisection approximation, which means that the cloud is approximated by two stacked cylinders of equal height. Finally, the Gaussian radial activity distribution at fixed heights in KDFOC3 are replaced by uniform distributions in NWSWAMP. Thus, in NWSWAMP the fully stabilized cloud is described as a collection of vertical cylinders, with uniform activity distributions, cf. Figure 34 above.

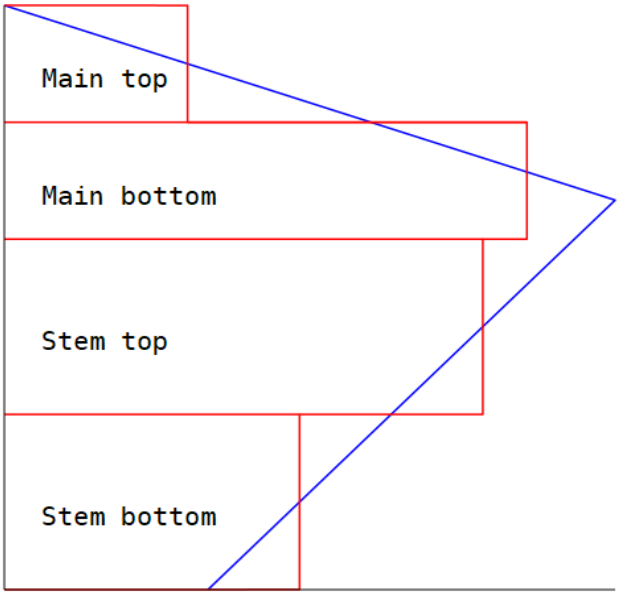


**Figure 37** NWSWAMP approximation (red curve) of a KDFOC3 vertical distribution (blue curve), for a surface burst (no base surge cloud.

We have the following correspondence between variables in the KDFOC3 report (Harvey *et al.*, 1992) and quantities in the description above:

**Table 4** Correspondence between notation in [1] and this report.

| KDFOC3 (Harvey *et al.*, 1992) | This report |
|---|---|
| $u_S, u_L$, p. 21 | $u_1, u_2$ |
| $wfa$, p. 46 | $A_{tot}$ |
| $ul_n$, p. 48 | $u_{1,n} = 1 - ul_n$, $u_{2,n} = ul_n$ |
| $z, zhat, zmin$, p. 52 | $\zeta = \frac{z}{zmax}, \hat{\zeta} = \frac{zhat}{zmax}, \zeta_{min} = \frac{zmin}{zmax}$ |
| $fzhat$, p. 53 | $\hat{\varphi}$ |
| $f_k(z)$, p. 53 | $\varphi_k(\zeta)$ |
| $AF_k(zb, zt)$, p. 53 | $I(\varphi, \zeta_b, \zeta_t)$ |
| $fr_{k,n}$, p. 54 | $u_{k,n}$ |
| $hq_{m,n} - hgz$, p. 54 | $\zeta$ |
| $hbs_n - hgz$, p. 54 | $\zeta_{b,n}$ |
| $hts_n - hgz$, p. 54 | $\zeta_{t,n}$ |
| $ATOT_k$, p. 54 | $Z_k$ |
| $AF_k(hbs_n - hgz, hts_n - hgz)$, p. 54 | $v_{k,n}$ |
| $wad_{d,n,k}$, p. 54 | $\varphi_k(\zeta; \zeta_{b,n}, \zeta_{t,n})/v_{k,n}$ |
| $\frac{wac_{k,n}}{wfa}$, p. 54 | $w_{k,n}$ |

## Nuclear Decision-Support System ARGOS

The Long-Range dispersion model interface in ARGOS has been developed in close cooperation with the different model providers through a number of years. The default interface is capable of handling forward deterministic Atmospheric Dispersion Modelling (ADM). In addition, specific interfaces have been developed for specific modelling needs such as handling ensemble calculations (developed in cooperation with DMI) and Adjoint modelling results (developed in cooperation with SMHI and SSM). Likewise, new interfaces will have to be developed in order to handle ADM from nuclear detonations. The implications of such interfaces will be discussed in this section.

### Nuclear Weapon Request Interface

Whereas the starting point for ADM-calculation for traditional nuclear and radiological releases is one or more single points where a time dependent source term is applied, the starting point for ADM from a nuclear detonation is – in this project (as we do not take modelling of the actual nuclear explosion into account) – a "stabilized cloud" that is the object for passive dispersion in the atmosphere.

The issue of determining such a stabilized cloud can be handled based on at least three different principles, and the actual implementation of the request interface can be based on each of these principles or combinations thereof. The principles are:

- The user provides the actual dimensions of the stabilized cloud: main cloud, stem and base surge. ARGOS sends these parameters to the ADM-model.
- The user provides a number of characteristics related to the nuclear explosion. Based on these characteristics ARGOS determines the cloud dimensions and sends these to the ADM-model.
- The user provides a number of characteristics related to the nuclear explosion, and ARGOS simply passes these on to the ADM-model. The ADM-model handles the calculation of the stabilized cloud itself.

The same principles can be applied for providing a source term for the nuclear explosion:

- The user provides the actual source term, and ARGOS sends the source term to the ADM-model.
- The user provides a number of characteristics related to the nuclear explosion. Based on these characteristics ARGOS determines the source term and sends it to the ADM-model.
- The user provides a number of characteristics related to the nuclear explosion, and ARGOS simply passes these on to the ADM-model. The ADM-model handles the calculation of the source term used.

An example of the latter can be seen below:

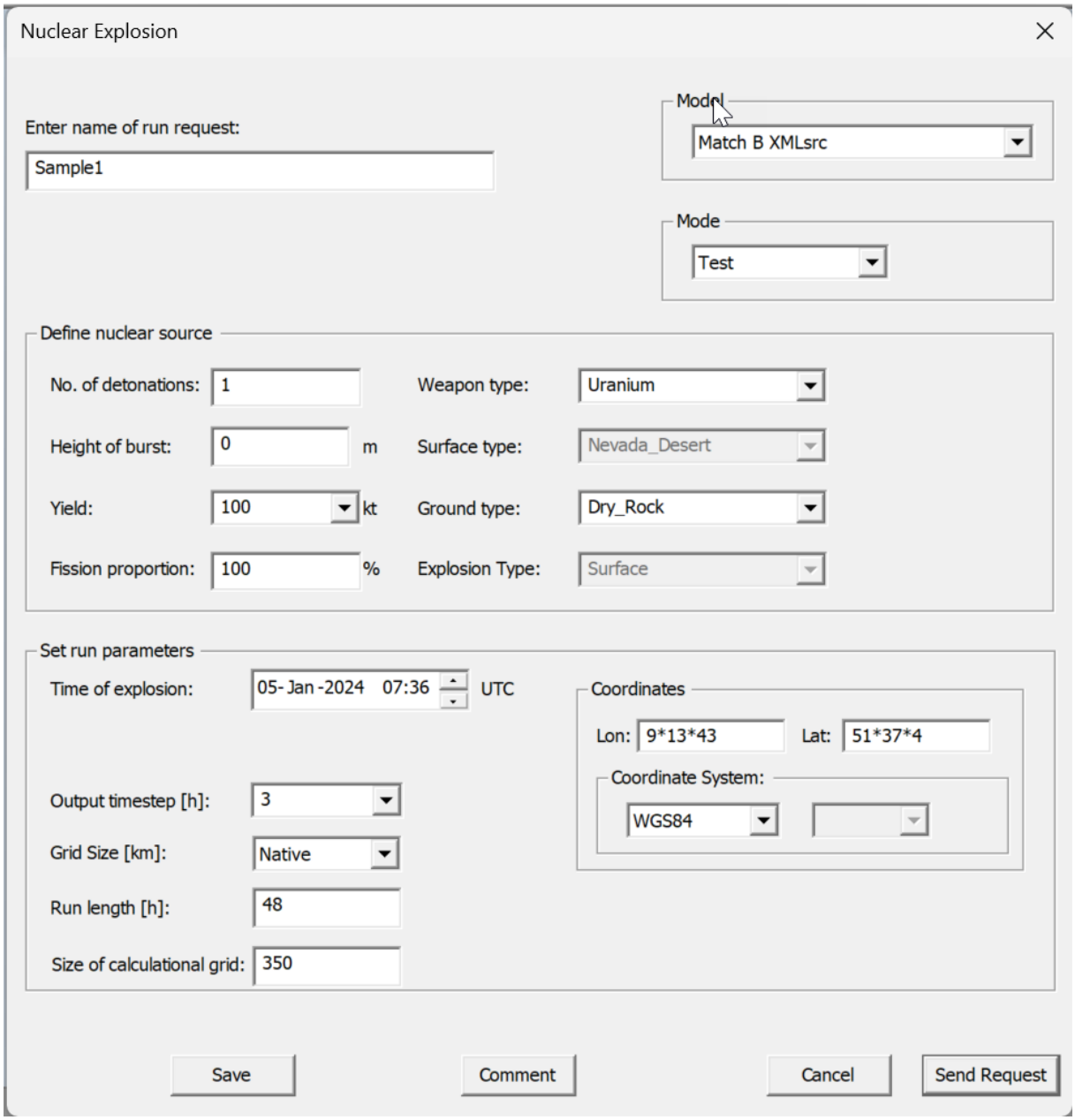


Where a set of characteristics for the nuclear explosion is determined by the user – seen in the "Define nuclear source section" – and ARGOS simply passes these parameters on to the ADM-model that then takes care of calculation of stabilized cloud as well as the source term. This interface requires that the receiving ADM-model has the necessary capabilities for performing these "pre-ADM" calculations. It should be noted that this solution prevents the user from having any direct influence on the determination of dimensions of stabilized cloud as well as the source term.

An example of a combination of bullet points one and two can be seen below:

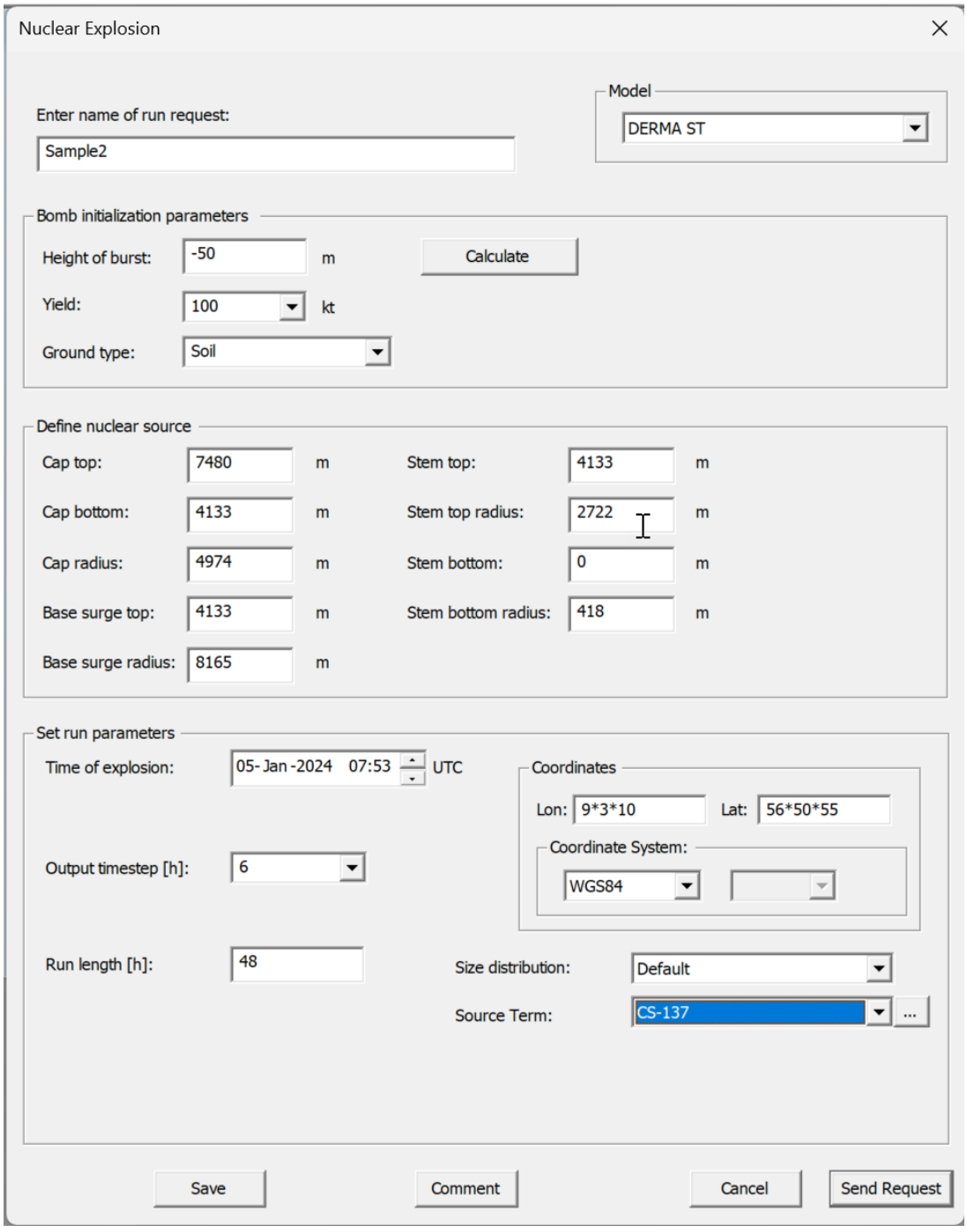


Here the user can in the first place provide a set of parameters for the explosion – in the "Bomb initialization parameters" section and the click Calculate. Based on these parameters ARGOS then determines the dimensions of the stabilized cloud – shown in the "Define nuclear source" section. In this case ARGOS is basing its calculations on the KDFOC3-model. Note that the user can examine and alter the individual cloud dimensions before sending them to the ADM-model. Lastly in this example the user directly determines the source term and the size distribution of the nuclides in the last part of the dialog.

## Dose Calculation and Presentation

A big issue in dealing with ADM-results based on nuclear explosions is the large number of nuclides, especially very short-lived nuclides, that is needed to represent the main contribution to the dose resulting from a nuclear explosion.

One solution to this problem is to simply use brute force and perform dose assessment for nuclear explosions in exactly the same way as it is done for (normal) nuclear and radiological releases, performing specific dose calculations for each individual nuclide in the specific run. Accepting that the dose assessment for hundreds of individual nuclides might be quite time consuming.

An alternative solution is to introduce the concept of pseudo nuclides where a single, or a very limited number of pseudo nuclides, represent the dose contribution of a larger set of individual nuclides. This approach obviously limits the number of calculations for activity and deposition on the ADM-model side but also the number of calculations needed on the dose assessment side, in ARGOS.

The concept of pseudo nuclide activity should be interpreted as bulk (gamma) activity – the activity of all the nuclides released in the explosion combined into one (or more) "pseudo-nuclide(s)".

The activity from the pseudo nuclides is anticipated to be presented to ARGOS from the ADM-model as the bulk gamma activity one hour after detonation. But the modelling start of nuclear explosions is not done at the moment of detonation, but rather at the time when a stabilized cloud prevails. This stabilized cloud constitutes the source term from a geometrical point of view.

The above is be taken into account when calculating the “decayed pseudo nuclide dataset”, presenting the basis for performing dose assessments in this situation.

A setting in ARGOS specifies the minutes between detonation and start of ADM, this setting is called FSC (Forming of Stabilized Cloud).

ARGOS will then use this information when calculating decayed pseudo nuclides.

Example:
If FSC = 10 mins then the time step T0 + 1 h in fact represents the time 1 h + 10 mins after detonation. In order to derive decayed pseudo nuclide activity for this time step, the pseudo nuclide activity should in fact be decayed by another 10 mins. Likewise, the time step T0 + 30 mins in fact represents the time 40 mins after detonation. In order to derive decayed pseudo nuclide activity for this time step, the pseudo nuclide activity should in fact be “undecayed” by 20 mins.

Decay of pseudo nuclides is handled with this formula:

$$A(t) = A(1)\, t^{-r},$$

where

| | |
|---|---|
| A(t): | Activity at time t [hours] |
| A(1): | Activity at t=1 [hours] |
| t: | Time after detonation [hours] – taking FSC into account |
| r: | Pseudo-nuclide Bomb Decay factor |

The decayed pseudo nuclides are then forming the basis for the actual dose calculations in ARGOS. When doing dose assessment in ARGOS based on pseudo nuclides only doses from deposition are taken into account. The Bomb decay factor as well as the so-called "Depo Gamma Factor" (Semi-infinite gamma radiation factor [Gy/s / Bq/m$^2$] for deposited material) for each pseudo nuclide needs to be provided as base data in the ARGOS-system. The specific values needed are typically derived from a practical approximation between ADM-runs with a full source term of "normal" nuclides and ADM-runs based on a source term of pseudo nuclide(s).

Below is an example of the "source term"-part of the ARGOS bomb request dialog using a pseudo nuclide, where ARGOS is calculating the "source term" for the pseudo nuclide based on bomb parameters:

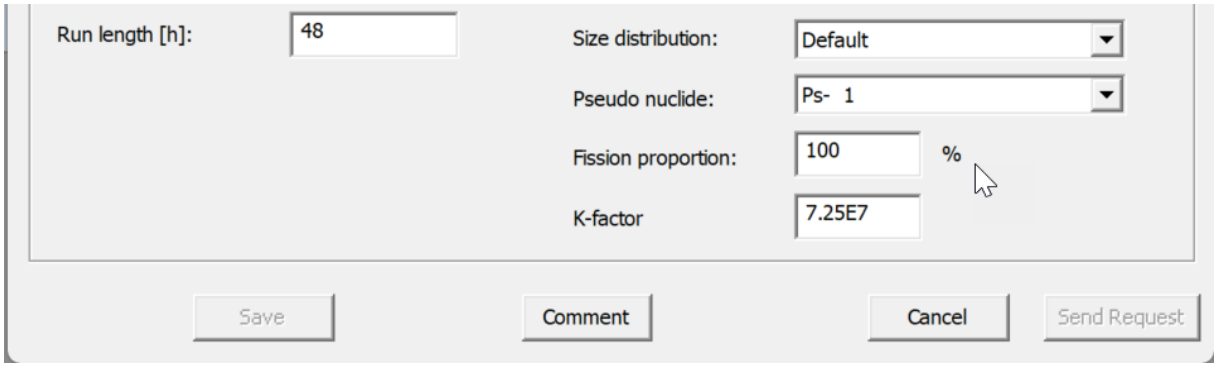


Compare to the normal source term request dialog in the section on Nuclear Weapon Request Interface. In this particular example the actual "source term", released activity of the pseudo nuclide again is calculated by ARGOS, using the KDFOC3-model and presented to the ADM-model as if it was a normal source term but just containing the selected pseudo nuclide and with all activity released with one minute.

### Vertical Distribution

For nuclear emergency preparedness and in associated decision-support systems, one typically presents calculated concentrations and doses at ground level since this level is of prime interest. However, especially for detonated nuclear weapons, large quantities of radioactivity may reside at high levels above ground, even up in the stratosphere, and it may be of interest to the experts guiding decision makers to have some knowledge on the position of the radioactivity aloft. Obviously, one may extend the concentration calculations to a number of vertical levels as it is usually done for calculation of volcanic ash concentrations in

case of volcanic eruptions. However, a simpler, and quicker approach, may be to simply plot the positions of particles or puff centres making up the three-dimensional model plume,

In Figure 38 an example of this is given. The total effective dose in Sv at ground level is shown as calculated by DERMA using Harmonie NWP model data. On top is plotted the positions of the centres of the puffs making up the model plume, the height of which is given in meters above ground. Note that the dose is a time-integrated quantity whereas the puff-centre positions are instantaneous.

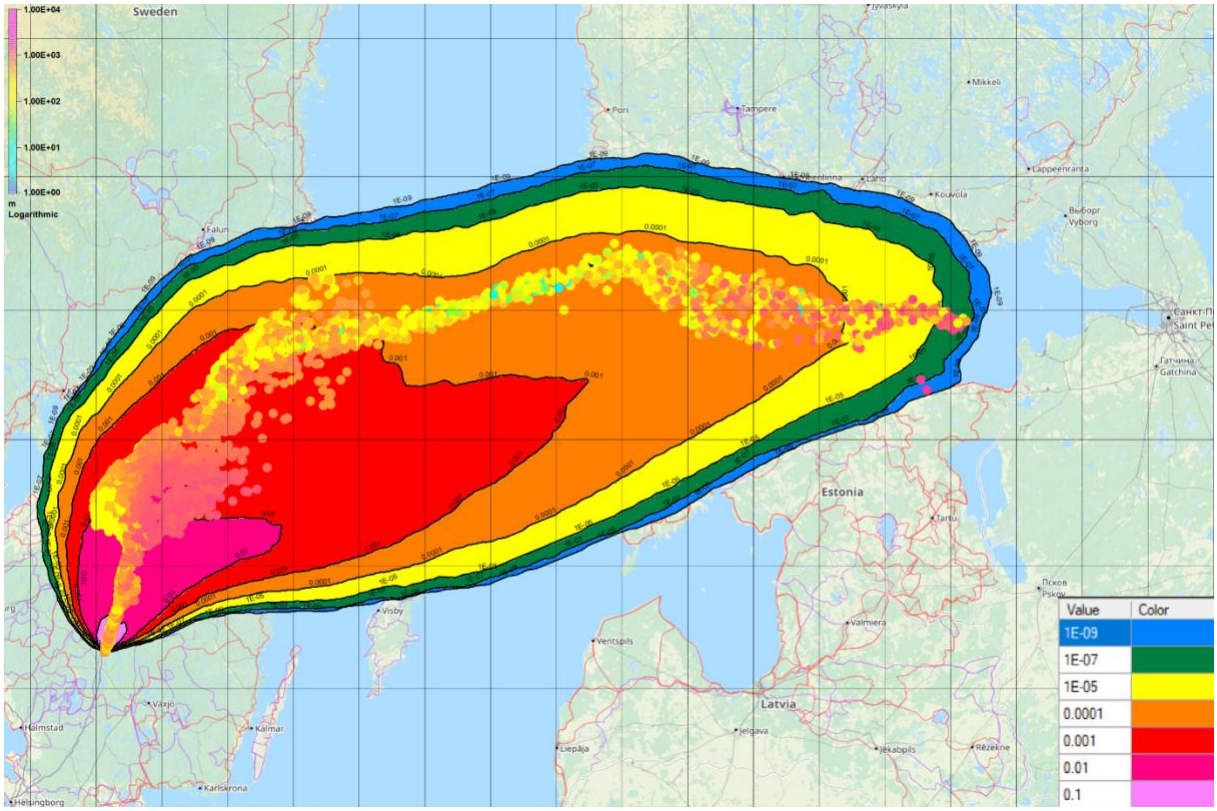


**Figure 38** Total effective dose in Sv at ground level according to the legend in the lower-right corner as calculated by DERMA using Harmonie NWP model data at 2.5 km horizontal resolution. On top is plotted the positions of the centres of the puffs making up the model plume, the height of which is given in meters above ground according to the logarithmic axis in the upper left corner.

## Meteorological Uncertainty

As shown by Sørensen *et al.* (2020) based on research carried out in the previous NKS-B projects MUD, FAUNA, MESO, and AVESOME (Sørensen *et al.*, 2014, 2016, 2017, 2019), the uncertainty of numerical weather prediction model data in use influences atmospheric dispersion modelling, and the corresponding uncertainty can be quantified by statistical ensemble methodology. Thus, also for the modelling of the dispersion of radioactivity from detonated nuclear bombs one can estimate the associated meteorological uncertainty. This can be illustrated e.g. in terms of percentiles of concentrations, depositions or dose rates, or in terms of probabilities for exceeding given threshold values, cf. Section “The Meteorological Ensemble” above, and especially Figure 14–Figure 24.

## Summary, Conclusions, and Outlook

In the DISARM project, studies have been carried out on existing descriptions of the initial spatial distribution of radioactive matter stemming from the detonation of a nuclear weapon. The selected description (KDFOC3), which is based on field observations of the dispersed radioactive cloud's geometrical shape, applies to the cloud once it is stabilized five to ten minutes after detonation, and the description is implemented as a pre-processor for atmospheric dispersion models taking over the stabilized cloud as the initial distribution of the tracers involved.

Case studies have been carried out involving different meteorological situations, weapon types and detonation heights. Corresponding to the meteorological cases, deterministic numerical weather-prediction (NWP) model data have been derived from the non-hydrostatic Harmonie model. Using these data, the atmospheric dispersion models DERMA and MATCH have been applied to the cases, and results derived and presented.

The previous NKS-B projects MUD, FAUNA, MESO, and AVESOME have demonstrated that in general case-dependent meteorological uncertainties play a significant role for the atmospheric dispersion modelling of radioactivity from an accidental release from a nuclear power plant. Similarly, since the meteorological uncertainties influence the transport pathway, they may have significant impact on emergency management far from the detonation of a nuclear weapon. Consequently, methods have been developed in DISARM and applied to the cases considered enabling quantification of the meteorological uncertainties of the predicted plumes. Comparisons are carried out of the effect of meteorological uncertainty on the dispersion on activity from a severe NPP accident and the detonation of a nuclear weapon at the same location.

An interface between a nuclear decision-support system and an atmospheric dispersion model has been developed and described. From either the geometrical field observations of the stabilized cloud, or from the yield in TNT equivalent as well as the height of burst, the interface calculates the parameters, which are required by the atmospheric dispersion model. These parameters are transferred to the dispersion model included in the request for dispersion calculation.

A study has been carried out on possibilities for improving the description of the initial phase, e.g. by incorporating dependences on meteorological parameters and arriving at better spatial distributions of radionuclides in the stabilized cloud and at descriptions of particle size distributions. Results have been obtained and presented.

The size distribution of particles resulting from detonation of a nuclear weapon plays a significant role. For instance, the fraction of large particles significantly influences the near field out to a couple of hundred kilometres from the location of the detonation. There are two effects: (i) the deposition pattern, and (ii) gravitational settling affecting the dynamics and thus also the transport pattern. The size distribution depends on the character of the explosion (free, surface, shallow, or deep burst) as well as on the nature of the ground affected by the fireball. There exist data on this from nuclear testing, but the knowledge is scarce involving e.g. only a limited range of different ground surfaces

A feasibility study has been carried out on the potential use of NATO standard messages in nuclear decision support systems. Such systems should preferably be able to accept NATO CBRN messaging according to e.g. the ATP-45 standard. Algorithms converting the information contained in these messages to the inputs needed for the atmospheric dispersion models are required thereby merging and co-processing multiple observation reports.

We have tested using the vorticity transport equation to model the development of the fireball arising from a nuclear weapon. The dimension of the stabilised cloud follows fairly well with the description in KDFOC3 for a 10 kt yield, while the vertical extent for a 100 kt yield is about 4 km lower than described in KDFOC3. The vertical extent increases though when a more accurate advection scheme is applied.

We have explored the article by Arthur *et al.* (2021) for separate modelling of the fireball from a vorticity transport model perspective. The width of the stabilised cloud arrives in the order described by KDFOC3 but the rise level does not reach the same level as described in KDFOC3. We have noticed though that our modelling gives a slower rise than shown by Arthur *et al.* (2021). Moreover, our simulations use about an hour of simulation time with a time step of a second. From an operational point of view, we may not foresee any practical use, but we may look further into self-induced precipitation that could be tabulated for operational applications.

## References


Andersson, C., Bergström, R., Bennet, C., Robertson, L., Thomas, M., Korhonen, H., Lehtinen, K.E.J., and Kokkola, H. 2015. MATCH-SALSA – Multi-scale Atmospheric Transport and CHemistry model coupled to the SALSA aerosol microphysics model – Part 1: Model description and evaluation. *Geosci. Model Dev.* **8**, 171–189. doi:10.5194/gmd-8-171-2015

Arthur, S.R., Lundqvist, K.A., Mirocha, J.D., Neuscamman, Kanarska, Y., and Nasstrom J.S. Simulating nuclear cloud rise within a realistic atmosphere using the Weather Research and Forecast model. *Atmos. Environ.* **254** (2021) 118363, 1-17.

Baker, G. H. Implications of Atmospheric Test Fallout Data for Nuclear Winter, report AD-A182607, Air Force Institute of Technology, Wright-Patterson Air Force Base, Ohio, U.S.A., 1987

Baklanov, A. and J. H. Sørensen. Parameterisation of radionuclide deposition in atmospheric dispersion models. *Phys. Chem. Earth* **26** (2001) 787–799

Bengtsson, L., U. Andrae, T. Aspelien, Y. Batrak, J. Calvo, W, de Rooy, E. Gleeson, B. H. Sass, M. Homleid, M. Hortal, K.-I. Ivarsson, G. Lenderink, S. Niemelä, K. P. Nielsen, J. Onvlee, L. Rontu, P. Samuelsson, D. S. Muñoz, A. Subias, S. Tijm, V. Toll, X. Yang, and M. Ø. Køltzow. The HARMONIE–AROME Model Configuration in the ALADIN–HIRLAM NWP System. *Monthly Weather Review* (2017) **145** No. 5 https://doi.org/10.1175/MWR-D-16-0417.1

Bouttier, F., Raynaud, L., Nuissier, O. and Ménétrier, B. (2016) Sensitivity of the AROME ensemble to initial and surface perturbations during HyMeX. *Quart. J. Roy. Meteor. Soc.* **142** 390-403, https://doi.org/10.1002/qj.2622

Daubechies, I. Ten Lectures On Wavelets. SIAM, 1992

Gloster, J., A. Jones, A. Redington, L. Burgin, J. H. Sørensen, R. Turner. International approach to atmospheric disease dispersion modelling. *Veterinary Record* 03 (2010a) **166** (12):369. DOI:10.1136/vr.166.12.369a

Gloster, J., A. Jones, A. Redington, L. Burgin, J. H. Sørensen, R. Turner, P. Hullinger, M. Dillon, P. Astrup, G. Garner, R. D'Amours, R. Sellers and D. Paton. Airborne spread of foot-and-mouth disease – model intercomparison. *Veterinary Journal* **183** (2010b) 278–286

Harvey, T., Serduke, F., Edwards, L., Peters, L. 1992, KDFOC3: A Nuclear Fallout Assessment Capability". Lawrence Livermore National Laboratory. UCRL-TM-222788

Hoe, S., J. H. Sørensen and S. Thykier-Nielsen. The Nuclear Decision Support System ARGOS NT and Early Warning Systems in Some Countries around the Baltic Sea. In:

Proceedings of the 7th Topical Meeting on Emergency Preparedness and Response, September 14–17, 1999, Santa Fe, New Mexico, USA

Hoe, S., H. Müller, F. Gering, S. Thykier-Nielsen and J. H. Sørensen. ARGOS 2001 a Decision Support System for Nuclear Emergencies. In: Proceedings of the Radiation Protection and Shielding Division Topical Meeting, April 14–17, 2002, Santa Fe, New Mexico, USA

Knox, J B. 1964. "Prediction of Fallout from Subsurface Nuclear Detonations". United States. https://doi.org/10.2172/4677749. https://www.osti.gov/servlets/purl/4677749.

Kraus, T. and Foster, K., 2014. Analysis of fission and activation radionuclides produced by a uranium-fuelled nuclear detonation and identification of the top dose-producing radionuclides. *Health Phys.* 107(2):150-63. doi: 10.1097/HP.0000000000000086.

Lindqvist, J. En stokastisk partikelmodell i ett icke-metriskt koordinatsystem., in: FOA-R-99-01086-862, FOA, 1999

Mikkelsen, T., S. Alexandersen, H. Champion, P. Astrup, A. I. Donaldson, F. N. Dunkerley, J. Gloster, J. H. Sørensen and S. Thykier-Nielsen. Investigation of Airborne Foot-and-Mouth Disease Virus Transmission during Low-Wind Conditions in the Early Phase of the UK 2001 Epidemic. *Atmos. Chem. Phys. Disc.* **3** (2003) 677–703

Molenkamp, C.R. Octet user's manual. National Laboratory. Technical Report UCRL-SM-226802. (2006)

Murray, F.W. Numerical models of tropical cumulus cloud with bilateral and axial symmetry. *Mon. Weath. Rev.* **98** No 1:14–28 (1970)

NATO Standard ATP-45. Warning and reporting and hazard prediction of chemical, biological, radiological and nuclear incidents. Edition F Version 2, March 2020

Ollinaho, P., Lock, S. J., Leutbecher, M., Bechtold, P., Beljaars, A., Bozza, A., Forbes, R. M., Haiden, T., Hogan, R. J. and Sandu, I. (2017). Towards process-level representation of model uncertainties: Stochastically perturbed parametrisations in the ECMWF ensemble. *Quart. J.* Roy. Meteor. Soc. 143 408–422, https://doi.org/10.1002/qj.2931

PDC-ARGOS. http://www.pdc-argos.com

Robertson, L., Langner, J. and Engardt, M., An Eulerian limited-area atmospheric transport model, *J. Appl. Met.* 38, 190-210, 1999

Sørensen, J. H. Sensitivity of the DERMA Long-Range Dispersion Model to Meteorological Input and Diffusion Parameters. *Atmos. Environ.* **32** (1998) 4195–4206

Sørensen, J. H., D. K. J. Mackay, C. Ø. Jensen and A. I. Donaldson. An integrated model to predict the atmospheric spread of foot-and-mouth disease virus. *Epidemiol. Infect.* (2000) 124, 577–590

Sørensen, J. H., C. Ø. Jensen, T. Mikkelsen, D. Mackay and A. I. Donaldson. Modelling the atmospheric spread of foot-and-mouth disease virus for emergency preparedness. *Phys. Chem. Earth* **26** (2001) 93–97

Sørensen, J. H., A. Baklanov and S. Hoe. The Danish Emergency Response Model of the Atmosphere. *J. Envir. Radioactivity* **96** (2007) 122–129

Sørensen, J. H., B. Amstrup, H. Feddersen, U. S. Korsholm, J. Bartnicki, H. Klein, P. Wind, B. Lauritzen, S. C. Hoe, C. Israelson, and J. Lindgren. Meteorological Uncertainty of atmospheric Dispersion model results (MUD). NKS-307, (2014) http://www.nks.org/en/nks_reports/view_document.htm?id=111010212220490

Sørensen, J. H., B. Amstrup, H. Feddersen, J. Bartnicki, H. Klein, M. Simonsen, B. Lauritzen, S. C. Hoe, C. Israelson and J. Lindgren. Fukushima Accident: UNcertainty of Atmospheric dispersion modelling (FAUNA). NKS-360 (2016), http://www.nks.org/scripts/getdocument.php?file=111010213440189

Sørensen, J. H., B. Amstrup, T. Bøvith, H. Feddersen, R. Gill, M. Sørensen, F. Vejen, P. Astrup, N. Davis, B. Lauritzen, S. C. Hoe, J. E. Dyve, P. Lindahl. MEteorological uncertainty of ShOrt-range dispersion (MESO). NKS-380 (2017) http://www.nks.org/en/nks_reports/view_document.htm?id=111010214043891

Sørensen, J. H., F. Schönfeldt, R. Sigg, J. Pehrsson, B. Lauritzen, J. Bartnicki, H. Klein, S. C. Hoe, and J. Lindgren. Added Value of uncertainty Estimates of SOurce term and Meteorology (AVESOME) – final report. NKS-420 (2019) http://www.nks.org/en/nks_reports/view_document.htm?id=111010214696230

Sørensen, J.H., Bartnicki, J., Blixt Buhr, A.M., Feddersen, H., Hoe, S.C., Israelson, C., Klein, H., Lauritzen, B., Lindgren, J., Schönfeldt, F., Sigg, R. Uncertainties in atmospheric dispersion modelling during nuclear accidents. *J. Environ. Radioact.* **222** (2020) 1-10 https://doi.org/10.1016/j.jenvrad.2020.106356

Winter, S., P.v. Schoenberg, L. Thaning, FOI Memo 2339. Utvecklingsarbete av systemet för spridningsberäkningar i den nationella strålskyddsberedskapen, in: FOI Memo 2339, Swedish Defence Research Agency FOI, 2008

## Appendix A - Derivation of the vorticity equation

The vorticity equation could be derived from the Navier-Stokes equation for momentum,

$$\frac{\partial \mathbf{v}}{\partial t} = -(\mathbf{v}\cdot\nabla)\mathbf{v} - \frac{1}{\rho}\nabla p + B\mathbf{k} + \nu\nabla^2\mathbf{v}$$

where the buoyancy term B is directed in the vertical (**k**) and defined by the density shift between the "bubble and the background,

$$B = -g\frac{\rho - \rho_b}{\rho}$$

where $\rho_b$ is the density of a background state. From the definition of vorticity

$$\underline{\omega} = \nabla \times \mathbf{v}$$

we may rewrite the momentum equation in the form

$$\rho\frac{\partial \mathbf{v}}{\partial t} = -\rho(\nabla\left(\frac{1}{2}|\mathbf{v}|^2\right) - \mathbf{v}\times\underline{\omega}) - \nabla p + B\mathbf{k} + \rho\nu\nabla^2\mathbf{v}$$

Note that $\underline{\omega}$ at this stage is a 3D vector. Then considering the vector relations

$$\begin{aligned}
\nabla^2\mathbf{v} &= \nabla(\nabla\cdot\mathbf{v}) - \nabla\times\underline{\omega} \\
\nabla^2\underline{\omega} &= \nabla(\nabla\cdot\underline{\omega}) - \nabla\times(\nabla\times\underline{\omega}) \\
\nabla\times(\mathbf{v}\times\underline{\omega}) &= (\underline{\omega}\cdot\nabla)\mathbf{v} - \underline{\omega}(\nabla\cdot\mathbf{v}) - (\mathbf{v}\times\nabla)\underline{\omega} + \mathbf{v}(\nabla\underline{\omega}) = \\
&= (\underline{\omega}\cdot\nabla)\mathbf{v} - (\mathbf{v}\cdot\nabla)\underline{\omega}
\end{aligned}$$

and taken the following constraints

$$\begin{aligned}
\nabla\cdot\mathbf{v} &= 0 \\
\nabla\cdot\underline{\omega} &= 0 \\
\nabla\times\nabla p &= 0
\end{aligned}$$

the curl of the momentum equation leads to

$$\frac{\partial \underline{\omega}}{\partial t} = -(\mathbf{v}\cdot\nabla)\underline{\omega} + (\omega\cdot\nabla)\mathbf{v} + \nabla\times B\mathbf{k} + \nu\nabla^2\underline{\omega}$$

The second term on the right hand side is a stretching term that disappears when we restrict our selves to consider the vorticity directed perpendicular to lateral-vertical plane (x; z), and the vorticity turn into a scalar entity. We may then rewrite to

$$\frac{\partial \omega}{\partial t} = -\mathbf{v}\nabla\omega + \frac{\partial}{\partial x}B + \nu\nabla^2\omega$$

The buoyancy could be rephrased in terms of potential temperature,

$$B = \frac{\theta - \theta_{bg}}{\theta_{bg}}$$

that lead us to the final form of vorticity equation for our purpose

$$\frac{\partial \omega}{\partial t} = -\mathbf{v}\nabla\omega + \frac{\partial}{\partial x}\frac{\theta - \theta_{bg}}{\theta_{bg}} + \nu\nabla^2\omega$$

Given the assumption that the wind **v** is the curl of a vector potential $\psi$

$$\mathbf{v} = \nabla \times \psi$$

we arrive at a Poissons equation for $\psi$

$$\omega = \nabla \times \nabla \times \psi = \nabla^2\psi$$

With the wind field we derive the evolution of potential temperature ($\theta$), the humidity ($q$), condensed water ($w$) and a virtual activity concentration ($c$),

$$\frac{\partial \theta}{\partial t} = -\mathbf{v}\nabla\theta + \nu\nabla^2\theta$$

$$\frac{\partial q}{\partial t} = -\mathbf{v}\nabla q + \nu\nabla^2 q$$

$$\frac{\partial w}{\partial t} = -\mathbf{v}\nabla w + \nu\nabla^2 w$$

$$\frac{\partial c}{\partial t} = -\mathbf{v}\nabla c + \nu\nabla^2 c$$

where the initial potential temperature and humidity is taken from HARMONIE weather data and the initial activity concentration having the same form as the initial potential temperature distribution,

$$c = \frac{c_{max}}{2}\left[cos(\frac{\pi r}{R}) + 1)\right]$$

Numerically we have adopted the above transport equations in flux form following Murray (1970).

**Acknowledgements**

NKS conveys its gratitude to all organizations and persons who by means of financial support or contributions in kind have made the work presented in this report possible.

**Disclaimer**

**Bibliographic Data Sheet** **NKS-498**

| | |
|---|---|
| Title | DISpersion of radioActivity fRom nuclear boMbs (DISARM) – final report |
| Author(s) | Jens Havskov Sørensen[1] (co-ordinator)<br>Kristian Holten Møller[1]<br>Kasper Skjold Tølløse[1]<br>Lennart Robertson[2]<br>Leif Å. Persson[3]<br>Daniel Vågberg[3]<br>Jan Pehrsson[4]<br>Henrik Roed[5]<br>Elias Pagh Senstius[5]<br>Naeem Ul Syed[6]<br>Anders Axelsson[7]<br>Anna Maria Blixt Buhr[7]<br>Jan Burman[3]<br>Jonas Lindgren[7]<br>Mikael Moring[8]<br>Tuomas Peltonen[8]<br>Mikko Voutilainen[8] |
| Affiliation(s) | [1]Danish Meteorological Institute (DMI)<br>[2]Swedish Meteorological and Hydrological Institute (SMHI)<br>[3]Swedish Defence Research Agency (FOI)<br>[4]PDC-ARGOS<br>[5]Danish Emergency Management Agency (DEMA)<br>[6]Norwegian Radiation and Nuclear Safety Authority (DSA)<br>[7]Swedish Radiation Safety Authority (SSM)<br>[8]Radiation and Nuclear Safety Authority (STUK) |
| ISBN | 978-87-7893-596-0 |
| Date | April 2025 |
| Project | NKS-B / DISARM |
| No. of pages | 62 |
| No. of tables | 4 |
| No. of illustrations | 41 |
| No. of references | 32 |

Abstract
max. 2000 characters

The current geopolitical situation implies an increased risk of use of nuclear weapons, the detonation of which can imply atmospheric dispersion of radioactivity posing a risk to the public also at long distances from the detonation. Thus, there is a need for developing new, or improving existing, model prediction tools for such events aiming at enhanced civil protection. Accordingly, the overall intention with the DISARM project was to improve the capability of predicting the atmospheric dispersion of radioactivity from nuclear explosions.

The model system describes the initial spatial distribution of radioactive matter when stabilization has occurred around ten minutes after the detonation. This effective initial spatial distribution will be taken over by an operational atmospheric dispersion model.

Existing descriptions and parameterizations based on parameters observed in the field have been studied and improved by incorporating recently developed dependences on meteorological parameters.

An interface to nuclear decision-support systems has been developed. From either field observations of the geometry of the stabilized cloud, or from the yield in TNT equivalent as well as the height of burst, the interface calculates the parameters, which are required by the atmospheric dispersion model. These parameters are transferred to the dispersion model included in the request for dispersion calculation.

Previous NKS-B projects have demonstrated that inherent case-dependent meteorological uncertainties play a significant role for the atmospheric dispersion model results. Corresponding methods are developed and applied to selected cases in order to quantify the meteorological uncertainties of the predicted radioactive plumes from nuclear explosions.

Key words

nuclear emergency preparedness, atmospheric dispersion modelling, nuclear weapons, detonation, stabilized cloud, particle size distribution